THE JOURNAL OF COMPARATIVE NEUROLOGY 431:363–381 (2001)

Evidence for Two Distinct Mechanisms of Neurogenesis and Cellular Pattern Formation in Regenerated Goldfish Retinas

DEBORAH L. STENKAMP,[1]* MAUREEN K. POWERS,[2] LAUREL H. CARNEY,[3] AND DAVID A. CAMERON[4]

[1]Department of Biological Sciences, University of Idaho, Moscow, Idaho
[2]Department of Cell and Molecular Biology, UC Berkeley, Berkeley, California
[3]Department of Biomedical Engineering, Boston University, Boston, Massachusetts
[4]Department of Physiology, Boston University School of Medicine, Boston, Massachusetts

ABSTRACT

After its destruction by intraocular injection of ouabain, the goldfish retina regenerates, but little is known about the histogenesis of the new tissue, including the structure and formation of regenerated cell mosaic patterns. In an effort to determine how retinal cells are generated and spatially organized within retina regenerated after ouabain injection, in situ hybridization and immunocytochemical techniques were combined with computational analyses of two-dimensional spatial patterns of identified neurons. Labeling with specific opsin riboprobes revealed two distinct cone patterns in the ouabain-injected eyes, each of which was different from the relatively orderly cone patterns of native retina. Central, regenerated regions had sparse aggregates of cones, and a relatively lower density of each cone type. Peripheral regions of experimental retina, likely derived from the circumferential germinal zone, had high densities of all cone types, each of which tended to be distributed randomly. The spatial patterns of inner retinal neurons in experimental eyes were also disorganized with respect to native retina. These results indicate that although some aspects of retinal regeneration resemble normal retinal development and growth, ouabain-induced regeneration does not produce well-organized mosaics of neurons, indicating a failure of the developmental interactions needed for proper pattern formation, which in turn could compromise visual recovery. Furthermore, the distinct cone patterns in different regions of experimental retina support the hypothesis that new goldfish retina arises via two spatially and cellularly distinct mechanisms after exposure to ouabain. J. Comp. Neurol. 431: 363–381, 2001.

Indexing terms: cone; photoreceptor; development; spatial pattern analysis; cone mosaic

The retinas of adult teleost fish, unlike those of amniote vertebrates, can regenerate neurons that are lost because of mechanical or chemical trauma (reviewed by Raymond and Hitchcock, 2000). For example, when a small piece of adult fish retina is surgically removed, a proliferative blastema forms along the lesion edge, which then generates new neurons (Hitchcock et al., 1992). Similarly, when the entire goldfish retina is destroyed subsequent to intraocular injection of the cytotoxic agent ouabain, regenerated retina is produced from spatially discrete neurogenic foci scattered throughout the damaged retina (Maier and Wolburg, 1979; Raymond et al., 1988). In both models, proliferative cells within the retina that survive the injury are believed to repopulate the damaged retina with new neurons (Raymond and Hitchcock, 2000).

Evidence suggests that the regenerative process in teleost retina may represent an injury-triggered recapitulation of developmental mechanisms. For example, the pro-

Grant sponsor: National Institutes of Health; Grant numbers: EY12146, EY03352, EY11160.

*Correspondence to: Deborah L. Stenkamp, Department Biological Sciences, University of Idaho, Moscow, ID 83844-3051.
E-mail: dstenkam@uidaho.edu

Received 29 August 2000; Revised 29 November 2000; Accepted 4 December 2000

liferative blastema (Hitchcock et al., 1992) expresses *vsx-1, pax6,* and *Notch,* genes known to be involved in retinal development (Levine et al., 1994; Hitchcock et al., 1996; Sullivan et al., 1997). Additionally, various structural features of the regenerated retina—including its lamination (Hitchcock et al., 1992), repertoire of cell types (Cameron and Carney, 2000), synaptic connectivity (Hitchcock and Cirenza, 1994; Hitchcock, 1997), and dendritic arborizations (Cameron et al., 1999)—imply the operation of normal (i.e., developmental) neurogenerative mechanisms.

Equally compelling evidence suggests, in contrast, that retinal regeneration is not a simple recapitulation of normal retinal development and growth. For example, insulin-like growth factors, which stimulate pluripotent cells of the circumferential germinal zone to proliferate, may not exert a similar influence on cells of the regenerative blastema (Boucher and Hitchcock, 1998). Furthermore, the spatial patterns of inner retinal cells in regenerated retina are consistently less orderly than their counterparts in native retina (Cameron and Carney, 2000). Abnormal patterns of cone photoreceptors (Braisted et al., 1994; Cameron and Easter, 1995), including atypical photoreceptor morphologies (Cameron and Easter, 1995; Cameron and Powers, 2000), have also been observed in regenerated retina.

Little is known about the mechanisms that regulate the formation of cell mosaics during retinal development and regeneration, nor about correlations between cone patterns and visual pigment expression in regenerated retina. In an effort to better understand the formation of cell mosaics and the regenerative process, we combined in situ hybridization and immunocytochemistry with quantitative analyses of two-dimensional spatial patterns in regenerated goldfish retina after ouabain-induced injury. We report the presence of two distinct cone patterns in these experimental retinas: a clumpy pattern that predominates in regenerated retina, and a near-random arrangement that typifies new peripheral retina. Each of these patterns is different from the regular, nonrandom mosaics of native retina, implying an absence or failure of the mechanisms that normally regulate cone pattern formation during retinal development and growth. The existence of distinct cone mosaic patterns in different regions of ouabain-treated retina indicates that the goldfish retina produces neurons via two spatially and cellularly distinct mechanisms after exposure to ouabain.

MATERIALS AND METHODS

Injections and tissue preparation

Goldfish (*Carassius auratus*), from 8 to 12 cm total body length, were purchased from Ozark Fisheries (Stoutland, MO) and maintained in 19- to 38-liter aquaria at 20°C. Fish were anesthetized in 0.1% tricaine methanesulfonate (MS-222; Sigma, St. Louis, MO). A small incision was made in the cornea with a microknife, then a blunt-end Hamilton (Reno, NV) syringe was introduced into the eye with a micromanipulator. To kill retinal cells and induce a regenerative response, 1–2 μl of 0.4 mmol/liter ouabain (Sigma) in sterile saline was injected into the left eye, to give an estimated intraocular concentration of approximately 30–50 μM (Maier and Wolburg, 1979; Raymond et al., 1988; Cameron and Powers, 2000). Right eyes were injected with identical volumes of sterile saline. To label proliferating cells, 0.5–2.0 μl of a 1.0 mmol/liter solution of 5-bromo-2′deoxyuridine (BrdU; Sigma) in sterile saline was injected into both eyes of one of the ouabain-treated fish, to give an intraocular concentration of approximately 50 μmol/liter. Fish were allowed to recover in small containers of aquarium water before being returned to their home tanks.

At 6, 8, or 11 months after ouabain injection (regeneration is considered complete by 2.5 months; Raymond et al., 1988), fish were anesthetized and decapitated; eyes were enucleated and lenses were removed. For whole-mount preparations intended for in situ hybridization, retinas were dissected from the eye, fixed for 1 hour in 4% paraformaldehyde in phosphate-buffered 5% sucrose (pH 7.4), washed with phosphate/sucrose, and stored in 100% methanol at −20°C (Raymond et al., 1993). Whole mounts to be used for immunocytochemistry were prepared as described previously (Cameron and Easter, 1995). Eyes intended for cryosectioning were processed according to Barthel and Raymond (1990) or Cameron and Easter (1995).

Immunocytochemistry and in situ hybridization

The primary antibodies used in this study were: zpr-1, a mouse monoclonal antibody previously known as FRet43, which labels a surface epitope on red/green double cones of zebrafish and goldfish (Larison and BreMiller, 1990; Schultz et al., 1997; Zebrafish Monoclonal Facility, University of Oregon, Eugene); anti-BrdU monoclonal antibody raised either in rat (Accurate Chemical, Westbury, NY) or mouse (Amersham, Arlington Heights, IL); mouse anti-tyrosine hydroxylase (Chemicon, Temecula, CA); rabbit anti-protein kinase C (Chemicon), rabbit anti-serotonin (Incstar, Stillwater, MN), and mouse anti-proliferating cell nuclear antigen (PCNA; BioMeda, Foster City, CA). Standard immunocytochemical procedures for indirect immunofluorescence were used (Knight and Raymond, 1993; Cameron and Easter, 1995; Cameron and Carney, 2000; Wan and Stenkamp, 2000). Cryosections intended for anti-BrdU or anti-PCNA immunocytochemistry were pretreated with a 1:1 solution of 2N HCl: phosphate-buffered saline (pH 7.4).

Goldfish opsin cDNA clones GFrod, GFred, GFgr-1, GFblu, and GFuv were gifts from K. Nakanishi (Columbia University) and F. Tokunaga (Osaka University) and correspond to the full-length coding sequences of the rod, red cone, green cone, blue cone, and ultraviolet cone opsins, respectively (Johnson et al., 1993; Raymond et al., 1993; Stenkamp et al., 1997). These were used to generate digoxigenin- or fluorescein- labeled cRNA antisense probes using the Genius System (Roche). Procedures for in situ hybridization on retinal cryosections and whole-mounts have been described (Barthel and Raymond, 1993; Raymond et al., 1993). Double in situ hybridizations were done using methods described by Stenkamp et al. (2000; see also Hauptmann and Gerster, 1994).

Photography

Most images were obtained using a Leica DMR microscope and a Spot camera (Diagnostic Instruments), under brightfield, epifluorescence, or Nomarski optics. In some cases, images obtained using different optical systems were combined using the "apply image" function in Adobe

Photoshop 4.0 (Adobe Systems, Mountain View, CA). Epifluorescence visualization and photography of inner retinal cells were performed with a Zeiss Axioskop and associated 35-mm camera system.

Computational analysis of cell patterns

The two-dimensional pattern of cone photoreceptor and inner retinal cell mosaics was examined by means of three independent analytical methods. For all methods, the starting material was a whole-mount preparation that had been hybridized to one or two of the goldfish cone opsin riboprobes or exposed to one of the primary antibodies, as described above. One or more 200-μm $\times$ 200-μm regions of each preparation were analyzed. Only regions free of overt tearing or mechanical distortion, and with cellular patterns judged to be representative of that particular retinal region, were selected for analysis. To meet such strict criteria, smaller regions were sometimes used (e.g., 150 μm $\times$ 200 μm). In all cases, the planimetric density of each cell type was estimated by dividing the number of labeled cells by the sampling area.

Nearest-neighbor distance analysis. Nearest-neighbor distance (NND) analysis is a technique used to characterize two-dimensional cell patterns, based on each cell's distance to the nearest neighboring cell, and was used here to determine whether cell patterns were nonrandom, and how well they compared to each other statistically (Wässle and Riemann, 1978; Cook, 1996). In each sampling area, individual labeled cells were assigned unique (x, y) coordinate values (using ScionImage software, Scion Corp.), and an NND for each cell was calculated using custom-built software (Cameron and Carney, 2000). The resultant distributions of NND values for each cell type in control and experimental retinas were evaluated for nonrandomness by calculating a conformity ratio (mean NND/SD) and referring to the Ready-Reckoner Chart of Cook (1996). The NND distributions were compared to each other with an F-test (to compare variances) and an independent t-test (to compare means; significance assigned at $P < 0.05$).

Density recovery profile analysis. Density recovery profile (DRP) analysis detects anticlustering phenomena within a two-dimensional pattern of cells, by calculating the density of cells in a sample as a function of annular distance from a central reference cell (Rodieck, 1991). Application of the DRP in this study was similar to that described previously (Cameron and Carney, 2000), with an extension of the software to permit two different labeled populations of cells within a sampling region to be compared against one another (i.e., cross-correlation), as described in Rodieck (1991).

Quadrat analysis. Quadrat analysis (see Chapter 3 of Grieg-Smith, 1964, and Chapter 6 of Ripley, 1981) can determine whether a two-dimensional pattern of objects within a sampling area is regular, clumped, or neither clumped nor regular (i.e., random). In contrast to NND, which is a local measurement of pattern, based on cell–cell distances, quadrat analysis can provide attributes of the more general and long-range pattern. In the present study, each sampled retinal area was subdivided into a grid of contiguous, square-shaped quadrats (boxes) of equivalent area, such that the sampled area was successively divided into $n = 4$, 9, 16, etc. quadrats, up to $n = 100$. For each n condition, the number of labeled cells within each quadrat was counted, the mean (x) and variance (s^2) computed, and an Index of Clumping (ICS; David and Moore, 1954; Ripley, 1981) was calculated as

$$\text{ICS} = (s^2/x) - 1.$$

ICS > 0 indicates a tendency toward an aggregated (clumped) pattern, ICS < 0 indicates a tendency toward a regular pattern, and ICS at or near 0 indicates a random pattern.

Significant differences from a random pattern were tested in two ways. First, the standard error for each ICS was determined, and for each ICS > 0, a t-test was used to evaluate whether ICS was significantly different from random (see p. 62 of Grieg-Smith, 1964). Because the t-test could only evaluate significance for values of the ICS > 0, an additional test of significance was used to confirm these results and evaluate ICS of any value. In this test, a statistical measure, termed an "index" of dispersion, $[(s^2/x) * (n - 1)]$, was referred to a χ^2 statistic at criterion $P = 0.05$, with $(n - 1)$ df (Skellam, 1952; David and Moore, 1954; Grieg-Smith, 1964). Any value of $[(s^2/x) * (n - 1)]$ *greater* than that expected for a Poisson (random) distribution indicates a clumped pattern that is significantly different from a random pattern, and any value of $[(s^2/x) * (n - 1)]$ *lower* than that expected for a Poisson distribution indicates a regular pattern (Grieg-Smith, 1964). Values of $[(s^2/x) * (n - 1)]$ that reside between the two "cutoff" levels in the χ^2 test "space" indicate patterns that are neither clumped nor regular (Figs. 5–7). A particular pattern of cells was judged to be clumped or regular if more than 50% of the $[(s^2/x) * (n - 1)]$ values were within that particular χ^2 test space.

Independent of the underlying pattern, for the t-test evaluation, significance ($P < 0.05$) was observed never to be achieved for $n < 9$, suggesting $n = 9$ as a lower limit for quadrat analysis (Grieg-Smith, 1964). Therefore, the index of dispersion values (χ^2 test) for $n < 9$ were excluded from the judgment of pattern type. However, for higher values of n (and for ICS > 0), the t-test evaluation and the χ^2 evaluation were always in agreement, and to simplify the graphical presentation of quadrat analysis, only the χ^2 analyses are illustrated in this report.

In some cases, the subdivided sampling regions from quadrat analysis were used to assess whether different cone types were associated with each other. In this analysis, presence or absence of each cone type within each quadrat was used to generate 2 $\times$ 2 contingency tables, and significance was assessed ($P < 0.05$) by calculating a χ^2 for the table (3 df; Grieg-Smith, 1964).

RESULTS

Description of intraocularly injected eyes

A total of 13 goldfish received intraocular injections of ouabain in their left eyes and saline in their right eyes; the experimental fates of these fish are shown in Table 1. The ouabain-injected eyes of 12 of the 13 fish had gross abnormalities that have been previously associated with retinal damage and a subsequent regenerative process, e.g., additional lenses, opacities in lenses and/or cornea (Mensinger and Powers, 1999). The other fish (Fish 6) displayed no such abnormalities, and on further dissection and analysis, the retina appeared not to have undergone a degenerative/regenerative process (see also Raymond et

TABLE 1. Retinal Preparations and Molecular Markers Used for Ouabain-Injected Goldfish

Fish	Survival time (mo)	Preparation	Markers	Comments
1	8	Cryosections	zpr-1; PCNA; GFrod; GFred/GFgr-1; GFblu/GFuv	Opaque cornea and lens
2	8	Whole-mount	GFred; GFblu	Opaque cornea and hypertrophied sclera
3	11	n/a	n/a	Two cataractous lenses
4	11	n/a	n/a	Opaque cornea
5	8	Whole-mount	GFgr-1; GFblu	Two clear lenses
6	6	n/a*	n/a*	
7	6	Whole-mount	GFblu/GFuv	Two clear lenses; opaque cornea
8	8	Whole-mount	GFblu	Two cataractous lenses
9	7	Whole-mount	GFgr-1; GFblu/GFuv	Opaque cornea
10	12	Cryosections	zpr-1; TH; PKC	Opaque cornea and lens
11	8	Whole-mount	TH	Two cataractous lenses; opaque material in retina
12	12	Whole-mount	PKC	Opaque cornea; no overt label in central retina
13	11	Cryosections	BrdU	Opaque cornea

n/a, not applicable because insufficient amount of regenerated retina was obtained; n/a*, not applicable because eye/retina appeared to be unaffected by the ouabain injection. TH, tyrosine hydroxylase; PKC, protein kinase C; BrdU, 5-bromo-2′-deoxyuridine.

al., 1988; Cameron and Powers, 2000). None of the saline-injected (henceforth termed "native") eyes displayed any abnormalities.

Of the affected 12 fish, 4 pairs of eyes were processed as cryosections, and 8 pairs of eyes were used to obtain whole-mounted retinal tissue. Two of these 8 eyes (from Fish 3 and 4; Table 1) were not suitable for further analysis either because no retinal tissue could be detected or because the small amount of regenerated retinal tissue obtained was insufficient for additional experiments. From some of these fish, whole mounts of retinas exposed to ouabain revealed two distinct regions that differed in their coloration and texture: a whitish, diffuse and in some cases delicate central region, and a gray–green peripheral region that resembled native retina in general appearance (Fig. 1). Although a precise boundary between these regions was not always apparent, they were sufficiently distinct to identify and analyze independently. The central region was ultimately interpreted as including retina regenerated from diffuse neurogenic foci, and will be referred to as "regenerated" retina, whereas the peripheral region was interpreted as containing retina produced from the circumferential germinal zone subsequent to ouabain exposure (Raymond et al., 1988; and see below), and will be referred to as "peripheral experimental" retina. Some native retinas were also subdivided (quartered) to test multiple cell markers on the same tissue.

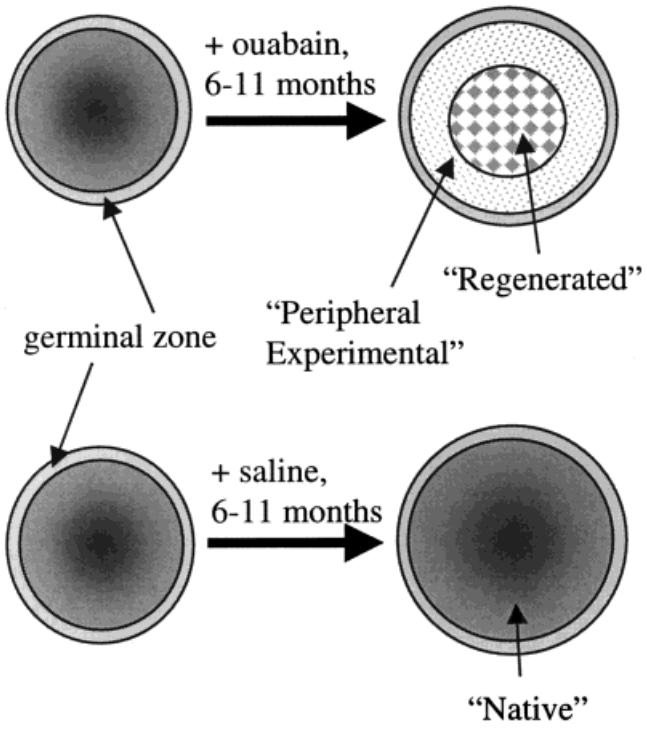

Fig. 1. Line drawing of retinas before and after ouabain/saline exposure. Ouabain-injected eye contains new retina derived from either surviving circumferential germinal zone ("peripheral experimental"), or regenerated from neurogenic foci ("regenerated") (Raymond et al., 1988). These regions were operationally defined, based on appearance and position of tissue, although a precise boundary was not always apparent. Saline-injected contralateral eye continues to develop new retina from the germinal zone; the entire retina is termed "native".

Two-dimensional patterns of cones in native retina

Because a detailed computational analysis of cone patterns in native goldfish retina has not yet been done, for each of the cell markers, the retinas from both experimental and control eyes were analyzed. Sectioned native retina showed labeling patterns for all markers (Fig. 2A,D,G,J) that were consistent with the analyses of native retina whole mounts (see below). Cones positive for the GFred and GFgr-1 probes (hereafter termed "red" and "green" cones, respectively) were the most abundant cone types (Fig. 2D), and a regular spacing of cones that were positive for GFblu ("blue" cones) and GFuv ("UV" cones) was evident (Fig. 2A). The cell-surface marker for red and green cones, zpr-1, revealed the characteristic morphology of teleost cone photoreceptors, with well-defined inner and outer segments and synaptic pedicles (Fig. 2G). Rod photoreceptors were abundant throughout the retina, with nuclei segregated in the innermost region of the outer nuclear layer (Fig. 1J; see Raymond et al., 1993).

Native retinal tissue, hybridized with a combination of GFblu and GFuv, displayed the typical lattice-like arrangement of blue and UV cones across the retinal sheet, but with some visible irregularities (Fig. 3A,B; see also Raymond et al., 1995; Stenkamp et al., 1996; Wan and

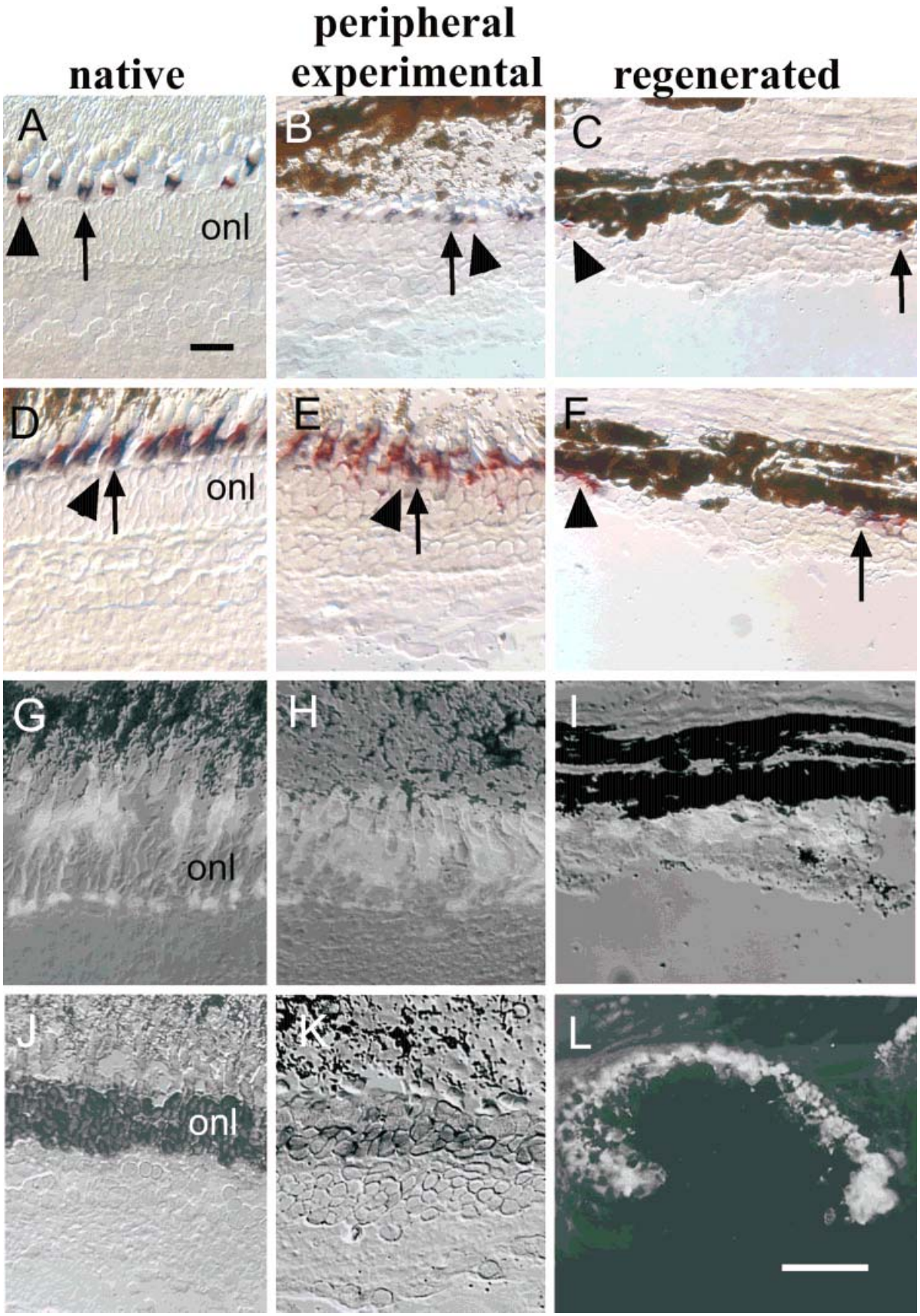

Fig. 2. Photoreceptor labeling of cryosections from native (A,D,G,J), peripheral experimental (B,E,H,K), and regenerated (C,F,I,L) goldfish retina. **A–C:** GFblu/GFuv double in situs; blue cones are labeled with dark blue color product (arrows); UV cones are labeled with the magenta color product (arrowheads). **D–F:** GFred/GFgr-1 double in situs; red cones are labeled with dark blue color product (arrows); green cones are labeled with the magenta color product (arrowheads). **G–I:** Indirect immunofluorescence with the red and green cone-specific zpr-1 antibody; labeled cells are brightly fluorescent. **J–K:** GFrod in situs. Rod cell bodies are labeled with the dark color product. **L:** Indirect immunofluorescence with zpr-1 on regenerated retina (different retina from the one shown in H and I). onl, outer nuclear layer. Scale bar = 50 μm (applies to all except L).

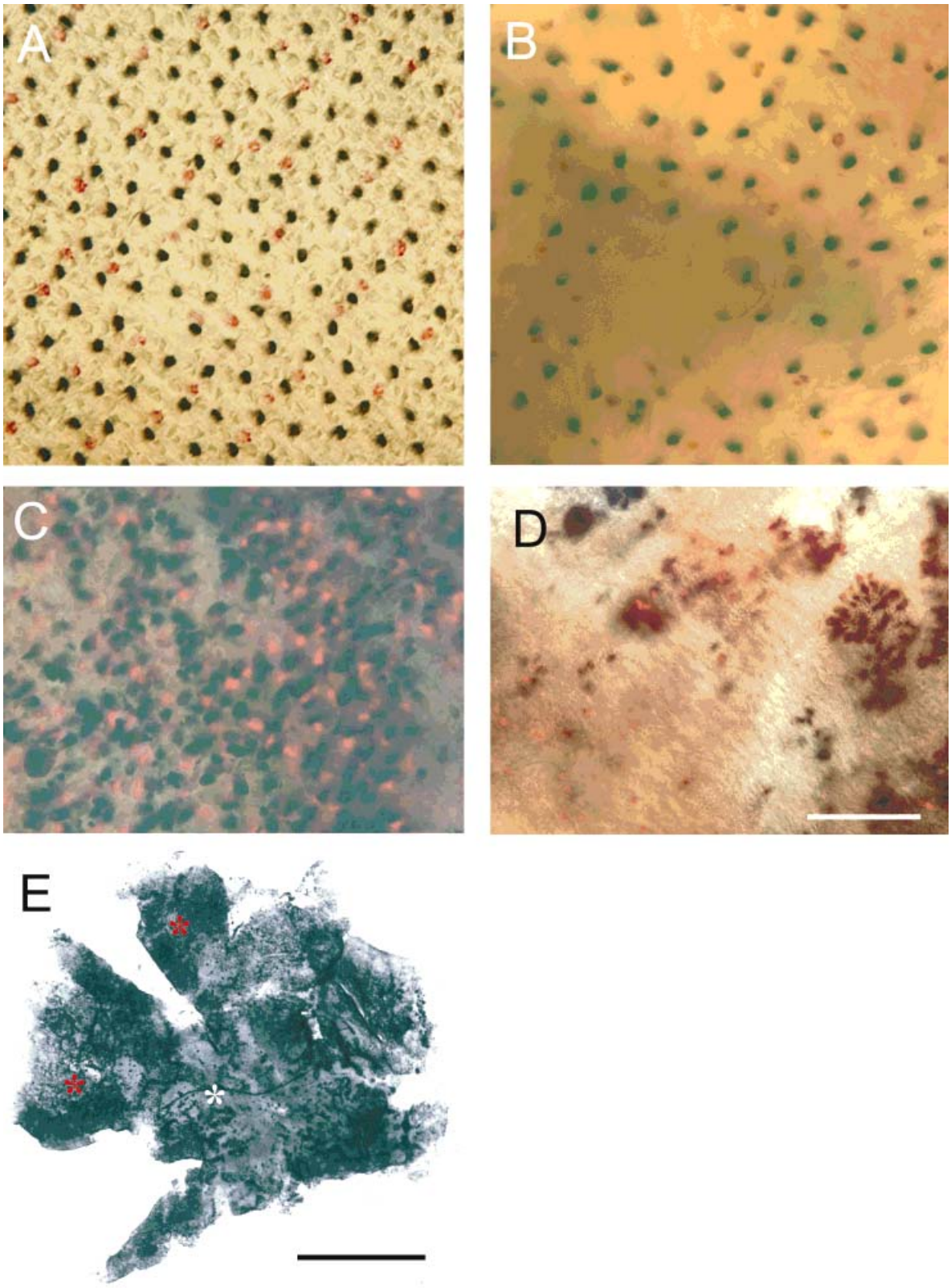

Fig. 3. A–D: GFblu/GFuv double in situs on native and experimental goldfish retina whole-mounts. Blue cones are labeled with dark blue color product; UV cones are labeled with the magenta/red fluorescent color product. Some images were obtained using a combination of brightfield and epifluorescence optics (the Fast Red color product is fluorescent). **A:** Native retina (Fish 9). **B:** Native retina; a region that reveals irregularities in the cone mosaic (Fish 7). **C:** Peripheral experimental retina (Fish 9). **D:** Regenerated retina (Fish 9). **E:** GFblu whole mount in situ of experimental retina (Fish 8); low-power view to show entire retina. Note densely labeled peripheral regions (red asterisks) and sporadically labeled central (regenerated) region (white asterisk). Scale bar = 50 μm in A–D; 1 mm in E.

TABLE 2. Cone and Inner Retinal Cell Arrangements in Native Goldfish Retina

Marker used	Fish	Cells/mm^2	$\bar{x}$ NND ± SD	NND-derived conformity ratio	DRP-derived effective radius	Pattern; derived from quadrat analysis[1]
GFred	2	7,775	7.9 ± 1.8	4.35*	4.7	Random
GFgr-1	5	5,575	10.2 ± 2.2	4.58*	8.4	Regular
GFgr-1	9	6,350	6.3 ± 2.8	2.30	3.6	Random
GFblu	2	4,075	12.0 ± 2.7	4.42*	11.5	Regular
GFblu	5	3,325	14.1 ± 2.2	6.46*	12.6	Regular
GFblu	7	1,925	17.6 ± 4.9	3.63*	15.5	Regular
GFblu	7	2,150	15.9 ± 5.1	3.13*	12.2	Regular
GFblu	9	3,950	13.9 ± 1.2	12.06*	12.4	Regular
GFuv	7	575	30.3 ± 7.2	4.23*	35.7	Random
GFuv	9	1,250	19.7 ± 5.9	3.32*	12.3	Regular
GFuv/ GFblu	7	N/A	9.4 ± 3.4	2.77*	b ➔ u, 6.4 u ➔ b, 6.4	n/a
GFuv/ GFblu	9	N/A	6.9 ± 1.4	4.90*	b ➔ u, 4.1 u ➔ b, 4.1	n/a
αTH	11	70	88.4 ± 21.9	4.04*	73.2	Regular
αPKC	12	1,135	23.0 ± 4.8	4.79*	18.2	Regular

[1]In this column, "regular," "clumped," and "random" were assigned, based on statistical difference ($P < 0.05$) from a random (Poisson) distribution and relative value of the ICS (see Figs. 5, 6, 8 and Materials and Methods). n/a, not applicable. b ➔ u, blue ➔ UV cones; u ➔ b, UV ➔ blue cones; NND, nearest-neighbor distance; DRP, density recovery profile; TH, tyrosine hydroxylase; PKC, protein kinase C.
[2]Meets Cook's (1996) criteria for a nonrandom distribution.

TABLE 3. Cone Ratios in Native and Experimental (Ouabain-Injected) Goldfish Retina

Fish	Ratio examined	Native	Peripheral experimental	Regenerated
2	Red:blue[1]	1.91:1	0.93:1	n/a
5	Green:blue[1]	1.68:1	1.3:1	2:1
9	Green:blue[1]	1.61:1	n/a	0.35:1
9	Blue:UV[2]	3.16:1	2.27:1	1.85:1

[1]Cone ratio estimated from cone densities measured in adjacent regions of the same retina, each hybridized with a single probe.
[2]Cone ratio calculated directly from double-hybridized material. n/a, not applicable; these combinations were not examined.

Stenkamp, 2000). Retinal tissue hybridized with GFred or GFgr-1 contained labeled cones that did not show a regular network, but did appear to be nonrandomly distributed (data not shown; see Raymond et al., 1995). Red and green cones were at the highest densities, followed by blue cones, then UV cones (Table 2). The ratios of blue:UV cones were calculated directly from double-hybridized material; however, other ratios were estimated from single-hybridized tissue from nearby regions of the same retina (Table 3), and these ratios were consistent with the findings of Marc and Sperling (1976) and Raymond et al. (1995).

The patterns formed by blue cones were analyzed from several native retinas (Table 2). These cones were chosen for a more extensive analysis than others because of their highly regular, lattice-like pattern. Also, the inner segments of blue-sensitive cones, where opsin mRNA is localized, are shorter than those of red or green cones, and are therefore visualized as spots on in situ hybridized whole mounts, rather than as extended bands of label (Raymond et al., 1993; Wan and Stenkamp, 2000), allowing less ambiguous identification of each cell's location.

Nearest-neighbor distance analysis. The hatched bars of Figure 4 show representative NND histograms for blue cones (Fig. 4A), UV cones (Fig. 4B), and UV-to-blue cones (Fig. 4C) in native retina; results obtained from additional retinas and additional cone types are summarized in Table 2. The NND distributions of native blue cones were consistently similar to normal (Gaussian) distributions, and the resulting conformity ratios easily met the criteria established by Cook (1996) for describing a nonrandom pattern, although mean NNDs were somewhat variable both between and within retinas (Table 2; see also Wan and Stenkamp, 2000). In contrast, the NND distributions for native UV cones showed complex bi- or trimodal distributions, likely because UV cones were frequently "missing" from their expected positions within the mosaic pattern (see also Stenkamp et al., 1996). However, NNDs between UV and blue cones were consistent, and the high conformity ratios indicated that these two cone patterns are correlated in native retina (Table 2). The observed patterns and NND distributions of red and green cones (the latter with one exception) were also regular, with high conformity ratios confirming that these cones had nonrandom mosaic patterns in native retina (Table 2).

Density recovery profile (DRP) analysis. The top row of Figure 5 shows a representative mosaic pattern of blue cones in native retina, along with the corresponding autocorrelation density recovery profile (DRP) and quadrat analysis (dispersion "index") plots. The top row of Figure 6 shows a similar presentation for a UV cone mosaic from a different native retina. The autocorrelation DRP analysis consistently revealed a zone of like-cone exclusion around each blue or UV cone (i.e., a nonzero "effective radius," Table 2; Rodieck, 1991), consistent with the anticlustering pattern that is evident from visual inspection. Additionally, the apparent periodicity in the "recovered" cone density values in each of the autocorrelation DRP plots was consistent with the regularity evident in both cone patterns, even though some UV cones were "missing" from the mosaic. The effective radius values derived from the autocorrelation DRP analysis were similar to the mean NND values (Table 2). Similar findings were obtained when autocorrelation DRP analysis was applied to red and green cone patterns in native retina, although periodicity in the recovered density profile was less pronounced (data not shown, effective radius values in Table 2).

Cross-correlation DRP for blue → UV and UV → blue cones indicated that the patterns of blue and UV cones were spatially correlated (Fig. 7), and the zone of unlike-cone exclusion surrounding each cone type was identical

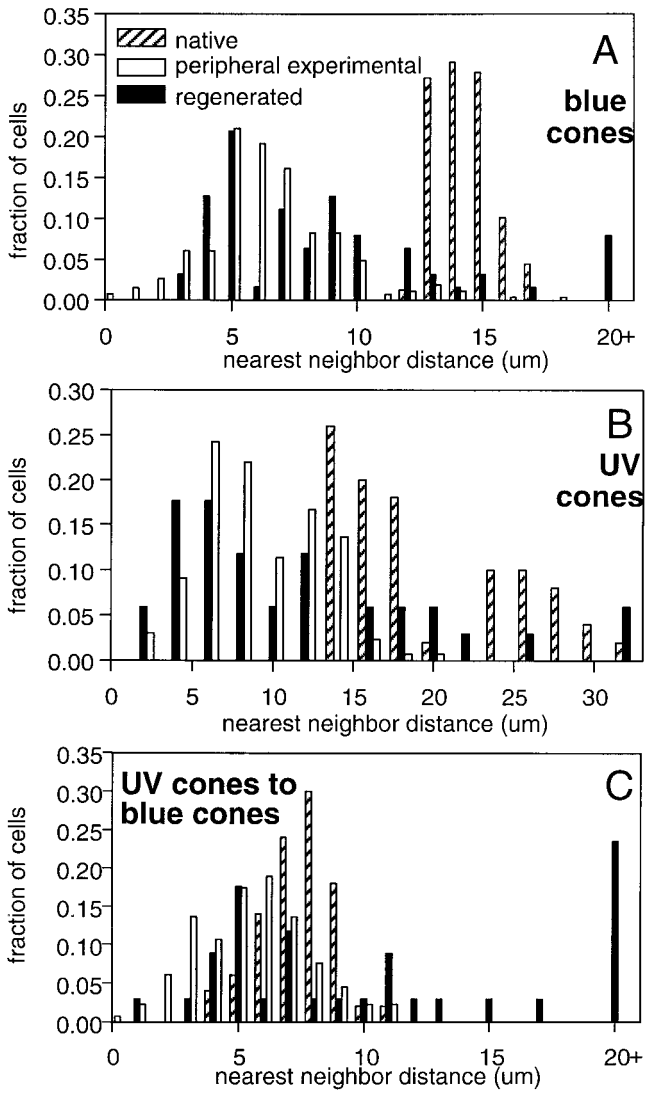

Fig. 4. Nearest-neighbor distance distributions of blue cones (**A**), UV cones (**B**), and UV-to-blue cone distances (**C**) in native retina (hatched bars), peripheral experimental retina (open bars), and regenerated retina (filled bars).

(effective radius values; Table 2). This result was expected for the lattice of blue and UV cones in native goldfish retina.

Quadrat analysis. Confirming the suggestion of the NND and DRP analyses, quadrat analysis revealed that the two-dimensional patterns were nonrandom *and* regular for blue and UV cones in native retina. The ICS values (see Materials and Methods) were consistently less than zero and, most importantly, the dispersion "indices" for these values were consistently less than that expected for random patterns; that is, dispersion indices were below the shaded regions of the rightmost panels in Figures 5 and 6, indicating that the patterns were statistically regular. With some exceptions, all cone mosaics in native retinas had similar spatial attributes by quadrat analysis, such that the patterns of all cone types were nonrandom and regular (Table 2; Fig. 8). In one example (Fish 7; Table 1), two regions of native retina were analyzed and showed only minor differences in blue cone pattern by all criteria used, suggesting little variation of cone pattern within intact retina.

These results provide a quantitative confirmation of earlier reports on cone mosaic patterns in goldfish retina (e.g., Marc and Sperling, 1976; Stell and Harosi, 1976), and they strongly suggest that the nonrandom and regular cone patterns must be assembled via some nonrandom spatial organization mechanism(s) during normal retinal development and growth.

Two-dimensional patterns of cones in experimental retina—general observations

Cone labeling in sectioned, ouabain-injected retina suggested that cones differed both in morphology and density, according to whether they were observed in peripheral or central regions of experimental retina. Specifically, a higher density of all cone types, but especially blue and UV cones, was found in the retinal periphery (Fig. 2B,E). Zpr-1 labeling in these peripheral regions showed that cone photoreceptors had fairly normal morphologies, although they were shorter and thicker than those in native retina. (Fig. 2H). Rod photoreceptors appeared to be less abundant than in native retina, but their cell bodies were properly positioned (Fig. 2K).

Cone patterns in (central) regenerated retina were atypical, and strikingly different from native retina. In the experimental retina that was processed for in situ hybridization and zpr-1 immunocytochemistry (Fish 1), centrally located photoreceptors were rare and had abnormal morphologies (Fig. 2C,F,I), reminiscent of the abnormal photoreceptor morphologies reported previously for ouabain-exposed retina (Cameron and Powers, 2000). Clearly identifiable regenerated retinal tissue was only rarely found at the posterior pole of cryosectioned experimental eyes, suggesting that robust regenerative responses may not always occur after ouabain exposure (see also Raymond et al., 1988). In the retina processed only with immunocytochemical markers (Fish 10), centrally located, regenerated photoreceptors were widespread, but frequently in abnormal positions (e.g., the retina displayed inverse polarity, and was poorly laminated; Fig. 2L). These zpr-1-positive cells also lacked identifiable inner and outer segments.

Preliminary examination of whole-mounted experimental retinas hybridized with GFblu confirmed the presence of two regionally distinct patterns: labeled cones were present at a relatively high density in peripheral regions, whereas central, regenerated retina contained a lower density of labeled cones, with a less uniform distribution (Fig. 3C,D,E). These distinctions were present regardless of survival time. Because of the two widely disparate patterns, wherever possible, the location of analyzed cell mosaics was assigned as "peripheral experimental" retina (i.e., proximal to the iris) or "regenerated" retina (i.e., proximal to the posterior pole). The computational analyses (below) were categorically segregated in this manner.

For each cone type examined in retinal whole mounts, NNDs were compared to data obtained from the contralateral control retina, using t-tests for means and F-tests for variances. In every case these differences were significant ($P < 0.05$), confirming that the cone distributions in experimental retina were different from those in native retina, and indicating a disruption in the spatial organiza-

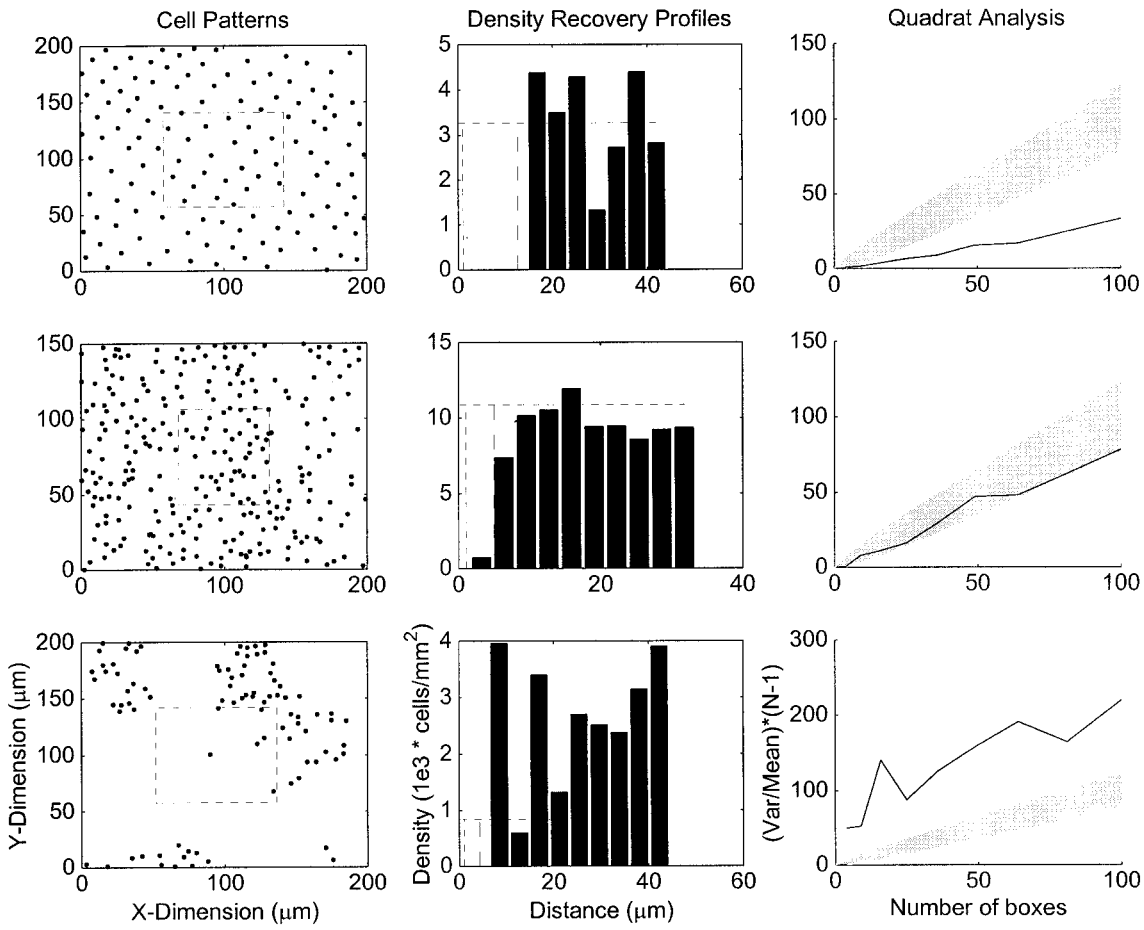

Fig. 5. Spatial patterns, density recovery profile (DRP) analysis, and quadrat analysis results for representative blue cone mosaics. The three rows of panels represent, from top to bottom, native, peripheral experimental, and regenerated retina. *DRP plots:* The bars on each DRP panel represent the "recovered" cellular density profile for the pattern displayed to the left, with the horizontal dashed line indicating the density of cells within the sampling box at the center of each pattern image. The leftmost vertical line on the plot (short dashed) indicates the estimated cone diameter, and the rightmost vertical line (long dashed) indicates the calculated effective radius (see Materials and Methods and Rodieck, 1991). The apparent periodicity in the "recovered" density profile for native retina is absent from peripheral experimental and regenerated retina. Additionally, compared to native retina, note the elevated density and lower effective radius for peripheral experimental retina, and the lower density, lower effective radius, and disrupted DRP of regenerated retina. *Quadrat analysis plots:* Each plot illustrates the dispersion "index" as a function of the number of quadrat boxes for the pattern to the left (see Materials and Methods). Dispersion "index" values above the shaded area indicate patterns that are statistically clumped, values below the shaded area indicate patterns that are statistically regular, and values within the shaded area indicate patterns that are neither clumped nor regular. Note that dispersion "index" values for each pattern display a consistent statistical trend as a function of quadrat box number, and that the statistical pattern determination matches that derived from visual inspection of the cone pattern.

tion mechanism(s) that operate in native retina. Although we did not routinely record the eccentricity of the control retinal regions used for these comparisons (i.e., central versus peripheral), cone pattern and density in intact, adult goldfish retina shows only minor variability (Marc and Sperling, 1976; see also Table 2, Fish 7). NNDs calculated for peripheral experimental retina were also statistically compared to NNDs obtained from central, regenerated retina in the same eye, and in nearly all cases these differences were significant.

Two-dimensional patterns of cones in experimental eyes—peripheral experimental retina

The densities of all cone types in peripheral experimental retina were significantly higher than those in native retina (Table 4). Ratios of red or green cones to blue cones were closer to 1:1 than to the characteristic 2:1 ratio in native retina (Table 3). The ratios of blue to UV cones were also different from those in native retina.

NND analysis. The open bars of Figure 4 illustrate the NND distributions for blue cones (Fig. 4A), UV cones (Fig. 4B), and UV-to-blue cones (Fig. 4C) in peripheral experimental retina. The NND distributions were generally less normal in shape than those of native retina, and for most cone types the mean NNDs were significantly lower. Compared to native retina, the conformity ratios (Cook, 1996) were also consistently lower for blue and UV cones, although in most cases they still met the criteria for a nonrandom distribution (Table 4). The conformity ratio for UV-to-blue cones in one example (Fish 9, Table 4; see also Fig. 4C) was also sufficiently high to suggest that, in

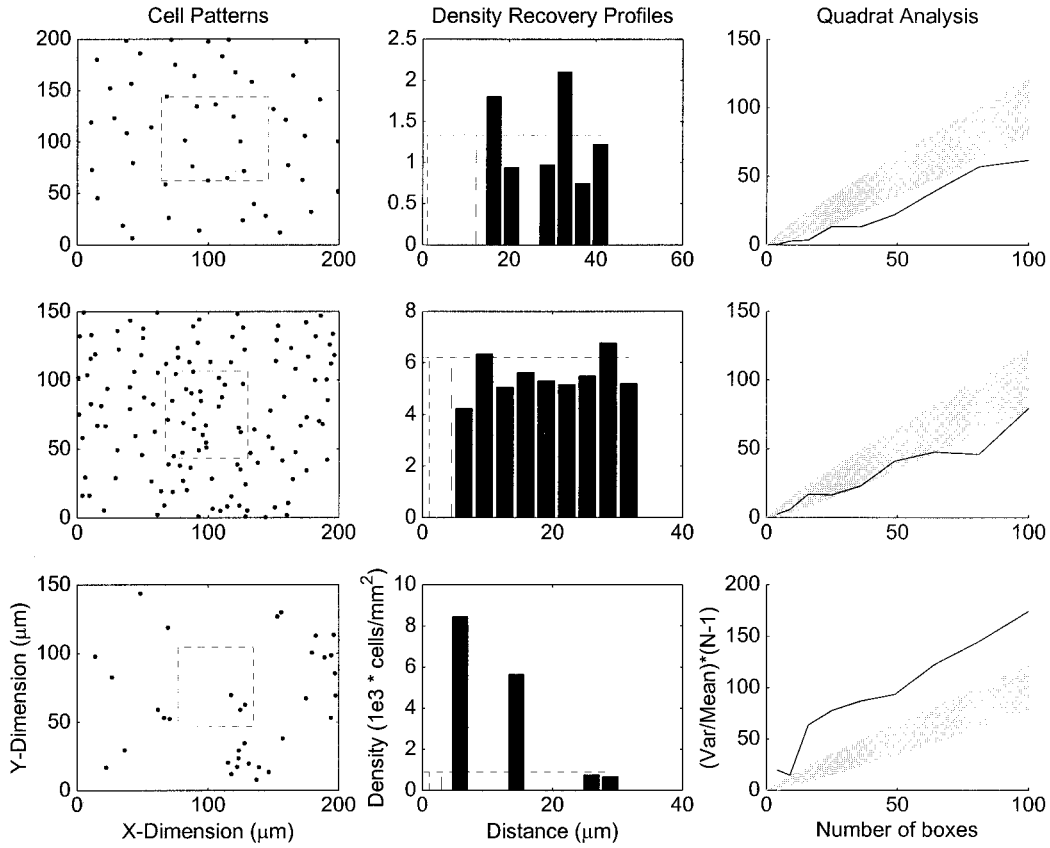

Fig. 6. Spatial patterns, density recovery profile (DRP) analysis, and quadrat analysis results for representative UV cone mosaics. The figure layout, and the information included in each DRP and quadrat analysis plot, are the same as in Fig. 5. Note that for each quantitative analysis, the trends in UV cone mosaic pattern, as a function of retinal condition, match those displayed by blue cones (Fig. 4).

peripheral experimental retina, these two cone types are spatially interdependent, as they are in native retina. However, an unidentifiable retinal region (that may have been peripheral) from this same experimental retina displayed a UV-to-blue cone NND conformity ratio that was quite low (Table 4), indicating that these two cone populations are not always spatially correlated. The NND distributions of red and green cones in peripheral experimental retina similarly had conformity ratios lower than their counterparts in native retina. These conformity ratio values, however, did suggest that these cone patterns were nonrandom (Table 4; Fig. 8).

DRP analysis. The middle rows of Figures 5 and 6 show, for blue and UV cones, respectively, representative cell patterns and the corresponding autocorrelation DRP and quadrat analysis plots for peripheral experimental retina. For both cone types, cone density in peripheral experimental retina was elevated compared to native retina (Table 4). The autocorrelation DRPs for both cone types revealed higher "recovered" densities than in native retina (consistent with the NND analysis and the directly measured density values; Table 4), and lower effective radius values (i.e., like-cell zones of exclusion) surrounding each cone. The latter result indicated a disruption in the anti-clustering phenomenon that characterizes cone mosaics in native retina. The apparent periodicity that was observed in the autocorrelation DRP plots of native retina was either suppressed or absent in the autocorrelation DRP plots for peripheral experimental retina, suggesting a lack of long-range periodicity in these cone patterns. Similar results were obtained for red and green cones in peripheral experimental retina (Table 4; Fig. 8). Cross-correlation DRP indicated that the effective radius values for blue → UV and UV → blue cones were not identical (Fig. 7; Table 4). Thus, the two cone types did not appear to be spatially correlated in peripheral experimental retina.

Quadrat analysis. The quadrat analysis plots in Figures 5 and 6 indicated that the mosaic patterns of blue and UV cones in peripheral experimental retina were neither regular nor clumped. The ICS values for these mosaics did not show any tendency toward values above or below zero (i.e., clumped and regular patterns, respectively) and in each dispersion index plot (e.g., the rightmost column of Figs. 5 and 6) the values resided within the shaded region, which indicates patterns that are neither clumped nor regular. With few exceptions, the quadrat analysis revealed similar attributes for the red and green cone photoreceptor patterns in peripheral experimental retina, namely, that most cone mosaics in peripheral retina were neither clumped nor regular (Table 4; Fig. 8). The apparent dichotomy between the NND and quadrat analyses—

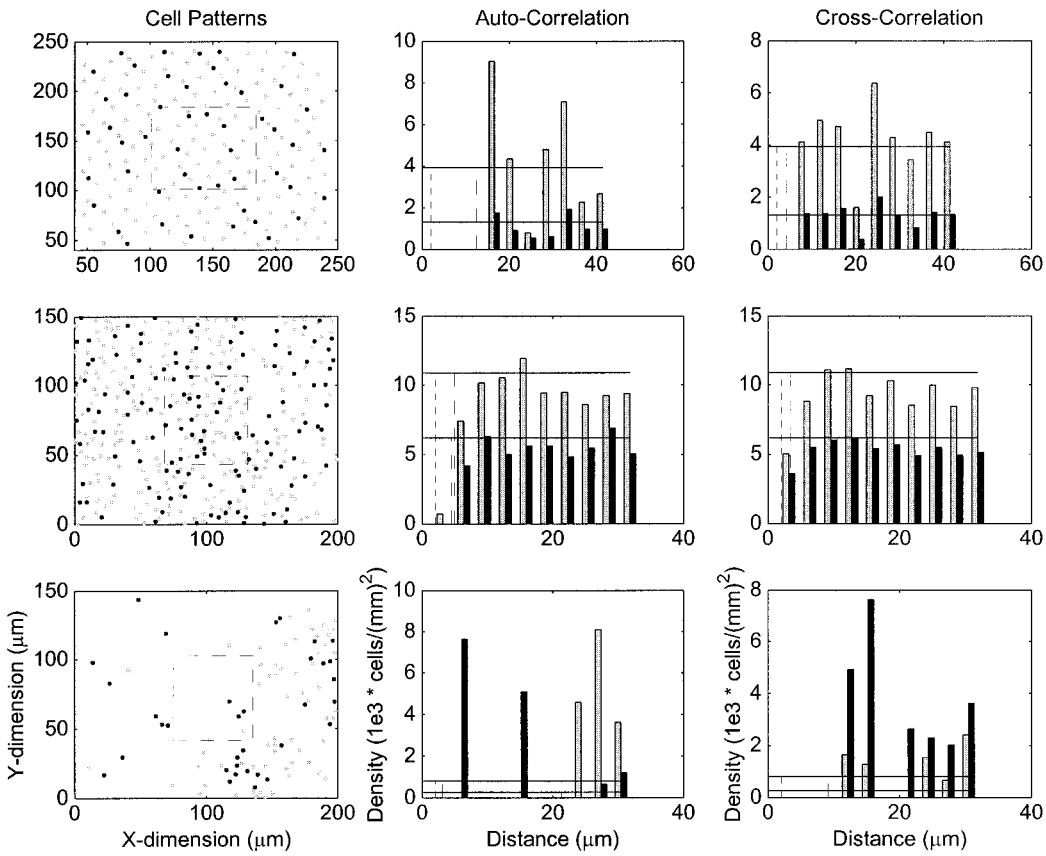

Fig. 7. Spatial patterns and density recovery profile (DRP) auto- and cross-correlations for representative mosaics of blue (filled symbols) and UV cones (open symbols). The three rows of panels represent, from top to bottom, native, peripheral experimental, and regenerated retina. *Autocorrelations:* In each plot, the DRP and effective radius values for blue (gray bars) and UV cones (black bars) are illustrated as in Figures 5 and 6. The "recovered" densities for the blue and UV cones are indicated by the upper and lower horizontal lines, respectively. Note that matching periodicity in recovered densities of blue and UV cones in native retina is not evident in either region of experimental retina. *Cross-correlations:* In each plot, the blue → UV cone condition is indicated by the solid bars, the UV → blue cone condition is indicated by the gray bars. The "recovered" densities are indicated as in the autocorrelation plots. Effective radius is indicated by the long-dashed vertical line, with the short-dashed vertical line indicating the estimated cone diameter. Note that the spatial correlation between blue and UV cones in native retina, as indicated by the lack of "recovered" density within approximately 5 μm of each cone, is compromised in peripheral experimental retina. The large effective radius values in regenerated retina could represent intercluster distances between the different cone types (see Results).

the NND results indicated regular patterns for peripheral experimental retina, whereas quadrat analysis suggested random patterns—may occur because NND analysis is, by definition, a *local* measure of mosaic pattern, whereas quadrat analysis involves a more spatially disperse analysis of the *entire* mosaic pattern.

Two-dimensional patterns of cones in experimental eyes—regenerated retina

The densities of all cone types in regenerated retina were generally lower than those in native retina (Table 4). Cone ratios revealed one example of the characteristic 2:1 ratio of green cones to blue cones, but another example of 0.35:1 (Table 3). The ratios of blue:UV cones were also different from those in native retina (Table 3).

NND analysis. The solid bars in Figure 4 illustrate representative NND histograms for blue cones (Fig. 4A), UV cones (Fig. 4B), and UV-to-blue cones (Fig. 4C) in regenerated retina. The NND distributions for these sampling areas were broader than those of native or peripheral experimental retina, and the resultant conformity ratios did not achieve Cook's (1996) criteria for a nonrandom pattern (Table 4). The conformity ratio derived from the UV-to-blue cone NND distribution was also quite low (Table 4), suggesting that in regenerated retina, these two cone patterns are spatially independent. The mosaic patterns of green cones in regenerated retina had similar NND distribution profiles and conformity ratios to blue and UV cones (Table 4; Fig. 8).

DRP analysis. The bottom rows of Figures 5 and 6 show, for blue and UV cones, respectively, representative cell patterns and the corresponding autocorrelation DRP and quadrat analysis plots for regenerated retina. The effective radius values derived from the autocorrelation DRP analyses were consistently smaller in regenerated retina than in native retina, indicating that the regenerated mosaic patterns did not possess the anticlustering attributes of their native retina counterparts. Additionally, the autocorrelation DRPs displayed dramatic, but nonperiodic, changes in like-cone density surrounding

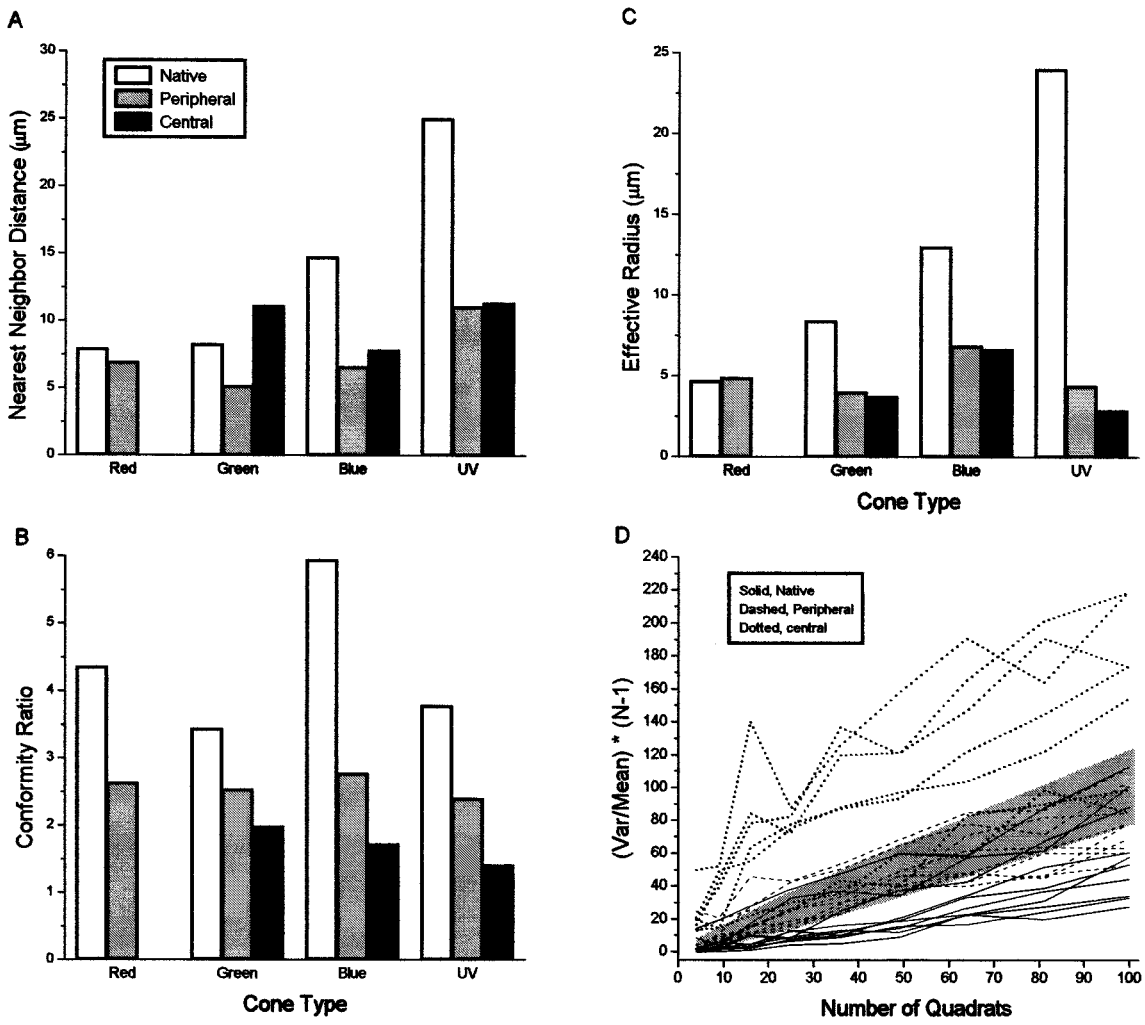

Fig. 8. Summary of quantitative mosaic pattern analyses for all cone types in native (open bars, solid lines), peripheral experimental (gray bars, dashed lines), and regenerated retina (solid bars, dotted lines). Data for red cones were unavailable for regenerated retina. **A:** Mean nearest-neighbor distance (NND) values. In almost all cases, the NND values in experimental retina were lower than those in native retina. **B:** Mean conformity ratio (CR) values (see Cook, 1996). In every case, the CR values in experimental retina were lower than the counterparts in native retina, indicating a trend toward randomness. **C:** Mean effective radius values derived from DRP analysis (see Rodieck, 1991). In nearly every case, the anticlustering attribute of native cone mosaics was disrupted in both regions of experimental retina. **D:** Dispersion "indices" derived from the quadrat analyses (see Materials and Methods), as a function of quadrat number. Native mosaics (solid lines) were nearly always regular, mosaic patterns in regenerated retina were nearly always clumped (dotted lines), and mosaic patterns in peripheral experimental retina were typically neither regular nor clumped (dashed lines).

each labeled cone, suggesting a clustering tendency within the sampled areas. The autocorrelation DRP analyses were similar for green cones in regenerated retina (data not shown; see Table 4 and Fig. 8 for effective radii). Lastly, cross-correlation DRP indicated that blue and UV cone patterns had no periodic attributes (Fig. 7). However, the effective radius values for blue → UV and UV → blue were identical (Table 4), suggesting the possibility of spatial correlation. Because the results from NND analysis and quadrat analysis (see below) do not support this interpretation, it is also possible that these effective radius values of the cross-correlation reflect zones of unlike-cone exclusion surrounding each *clump* of cones of a specific type, rather than zones of unlike-cone exclusion surrounding each *individual* cone.

Quadrat analysis. The quadrat analysis plots in the bottom rows of Figures 5 and 6 indicate that the patterns of blue and UV cones in regenerated retina were significantly different from those of native retina (cf. the top and bottom quadrat analysis plots in Figs. 5 and 6). Moreover, the ICS values for these mosaics were consistently greater than zero (data not shown), and the resultant dispersion "indices" were, with only one exception, consistently greater than those expected for a random pattern. These data indicate that the cone patterns in regenerated retina were significantly clumped, and thus were significantly different from the cone patterns of both peripheral experimental and native retina (Table 4).

To determine whether blue and UV cones were associated with each other *within* clumps, the presence or ab-

TABLE 4. Cone Photoreceptor Arrangements in Experimental (Ouabain-Injected) Goldfish Retina

Marker used	Fish	Region of experimental retina[1]	Cells/mm^2	$\bar{x}$ NND ± SD	NND-derived conformity ratio	DRP-derived effective radius	Pattern; derived from quadrat analysis[2]
GFred	2	Peripheral	8,225	6.9 ± 2.6	2.63[3]	4.9	Random
GFgr-1	5	Peripheral	11,750	5.1 ± 2.0	2.53[3]	4.0	Clumped
GFgr-1	5	Regenerated	1,650	6.8 ± 3.1	2.15	3.6	Clumped
GFgr-1	9	Regenerated	1,100	15.4 ± 8.4	1.8	3.9	Random
GFblu	2	Peripheral	8,825	6.5 ± 2.4	2.63[3]	6.0	Random
GFblu	5	Peripheral	9,025	6.6 ± 1.7	3.83[3]	4.3	Random
GFblu	5	Regenerated	825	7.0 ± 3.0	2.35	7.2	Random
GFblu	5	Unknown (r)	1,600	7.3 ± 5.4	1.34	3.7	Clumped
GFblu	7	Peripheral	8,400	6.4 ± 2.8	2.29[3]	12.2	Random
GFblu	7	Regenerated	2,250	6.9 ± 3.6	1.93	4.2	Clumped
GFblu	9	Peripheral	4,150	6.8 ± 2.9	2.31[3]	5.0	Random
GFblu	9	Regenerated	3,150	9.4 ± 11.8	0.84	8.6	Clumped
GFblu	9	Unknown (p)	6,675	6.0 ± 2.6	2.35[3]	1.2	Random
GFuv	9	Peripheral	1,825	11.0 ± 4.6	2.40[3]	4.4	Random
GFuv	9	Regenerated	1,700	11.3 ± 8.0	1.41	2.9	Clumped
GFuv	9	Unknown (p)	3,300	8.8 ± 3.6	2.49[3]	2.2	Random
GFuv/ GFblu	9	Peripheral	n/a	5.0 ± 2.2	2.34[3]	b ➜ u, 10.5 u ➜ b, 3.3	n/a
GFuv/ GFblu	9	Regenerated	n/a	13.4 ± 12.8	1.04	b ➜ u, 9.5 u ➜ b, 9.5	n/a
GFuv/GFblu	9	Unknown (p)	n/a	9.2 ± 7.1	1.29	n.d.	n/a
αTH	11	Peripheral	155	49.4 ± 18.1	2.73[3]	31.6	Random
αPKC	12	Peripheral	5,240	10.8 ± 2.2	4.91[3]	8.1	Regular

[1]Experimental retinal regions that were not conclusively identified as peripheral experimental or regenerated retina were tentatively categorized according to the results of quadrat analysis: r, regenerated; p, peripheral.
[2]In this column, "regular," "clumped," and "random" were assigned, based on statistical difference ($P < 0.05$) from a random (Poisson) distribution and relative value of the Index of Clumping (see Figs. 5, 6, 8). n/a, not applicable. n.d., this analysis was not done; NND, nearest-neighbor distance; DRP, density recovery profile; b ➜ u, blue ➜ UV cones; u ➜ b, UV ➜ blue cones; PKC, protein kinase C.
[3]Meets Cook's (1996) criteria for a nonrandom distribution.

sence of each cone type within each quadrat was used to generate 2 × 2 contingency tables, and significance was assessed by a χ^2 analysis (see Materials and Methods). This analysis revealed no significant association between blue and UV cones within clumps, providing additional confirmation that the distribution of cone types was independent of other cone types in regenerated retina.

Figure 8 summarizes analytical results for each cone type in each retinal region examined. Average NND values for all cone types were generally lower in peripheral experimental and regenerated retina than in native retina, in part because of higher cone densities in peripheral experimental retina and within clumps of cones in regenerated retina. However, conformity ratios displayed a consistent pattern: values for native retina were greatest, followed by those for peripheral experimental retina, followed by those for regenerated retina (Fig. 8B), reflecting decreasing regularity in pattern. Effective radius values tended to be larger in native retina than in peripheral experimental or regenerated retina (Fig. 8C). Lastly, quadrat analysis results for all regions (and all cone types) included in this study revealed consistently clumped patterns for regenerated retina, predominantly random (or near-random) patterns for peripheral experimental retina, and mostly regular patterns for native retina (Fig. 8D).

Two-dimensional patterns of inner retinal neurons in native and regenerated retina

Neurons in inner retina were also analyzed in either sectioned or whole-mounted retinal tissue, using immunocytochemical markers against tyrosine hydroxylase (TH, which labels interplexiform cells; Yazulla and Zucker, 1988), serotonin (which labels a subgroup of amacrine cells; Dowling, 1987), or protein kinase C (PKC, which labels a subpopulation of bipolar cells; Suzuki and Kaneko, 1990).

Cells that were immunopositive for TH and those immunopositive for serotonin were located in the appropriate retinal layer in both native and experimental retina (Fig. 9a and c; data not shown for peripheral experimental retina). However, the distribution of these cell groups in both peripheral experimental and regenerated retina was unusual. In regenerated retina, cells that were immunopositive for either TH (Fig. 9b) or serotonin (Fig. 9c) were generally positioned within tissue expanses that contained no recognizable retinal landmarks or laminae, or in "apical" regions of retinal tissue showing inverse polarity (Fig. 9b; this same retina, from Fish 10, was used for zpr-1 immunocytochemistry, Fig. 2L). Regenerated retina showed significant variability in lamination in the three cases in which cryosections were examined (Table 1), although it was occasionally well laminated, with three distinct cellular layers present (see Fig. 11b, and below). However, it could also display inverse polarity (e.g., Figs. 2L and 9b), contain a mass of retinal cells with no evidence of lamination (e.g., Fig. 9d), or consist simply of a small number of cells that express photoreceptor markers (see Fig. 2C,F,I).

The two-dimensional patterns of inner retinal cells in native and experimental tissue were pursued using the markers against TH and PKC. In native retina, there was an apparently homogeneous distribution of both cell groups across the retinal sheet, with cells immunopositive for PKC (Fig. 9g) having a higher density than those cells immunopositive for TH (Fig. 9e). NND analysis confirmed that both cell types were arranged in nonrandom patterns (Fig. 10; Table 2), and this conclusion was further supported by autocorrelation DRP and quadrat analyses (Fig. 10; Table 2).

In peripheral experimental retina, the planimetric densities for the two cell groups (TH, Fig. 9f; PKC, Fig. 9h) were higher than the corresponding densities in the con-

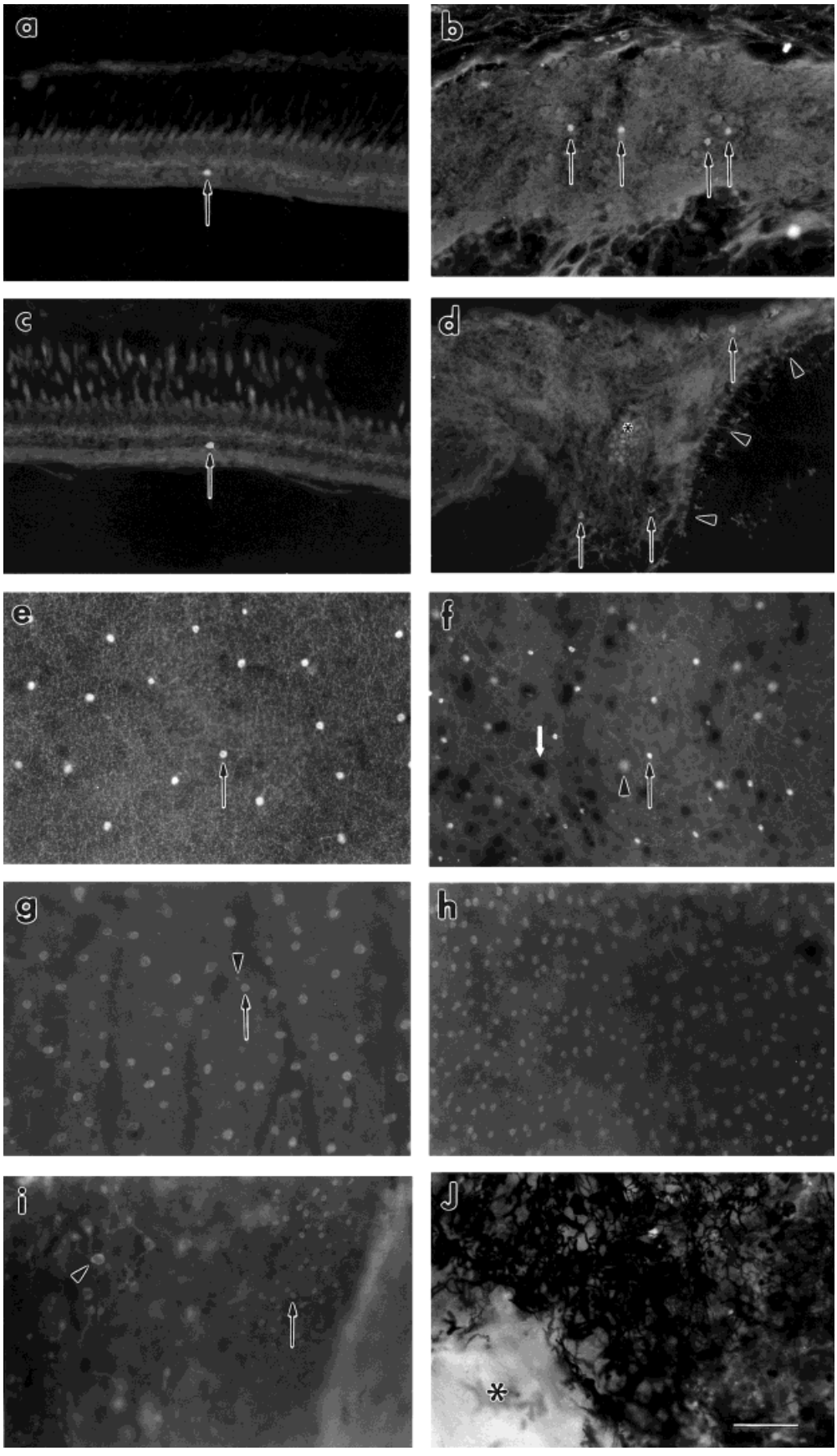

Figure 9

tralateral native retinas (cf. Tables 2 and 4). The NND analysis revealed significantly lower mean values in peripheral experimental retina (Fig. 10), but the attendant conformity ratios achieved Cook's (1996) criteria for a regular distribution. Quadrat analysis confirmed the regular pattern for cells that were immunopositive for PKC, but suggested a random pattern for cells that were immunopositive for TH. Additionally, in peripheral experimental retina, cells immunopositive for TH were frequently not coplanar, indicating yet another abnormality in their spatial distribution (Fig. 9f).

In regenerated retina, cells that were immunopositive for PKC were less densely arrayed (with interspersed regions of higher density), and these cells were not always localized within the same focal plane (Fig. 9i). The regenerated retina that was processed for the TH marker was difficult to analyze because it contained an opaque material (asterisk, Fig. 9j) that was surrounded by a plexus of heavily pigmented, fibrous structures: the immunopositive cells, if present, could not be resolved. In both cases, the size of regenerated retina that contained immunoreactive cells was insufficient for quantitative analysis.

Proliferative cells in experimental retina

To determine whether experimental retina contained cell populations that could continue to generate new retinal neurons, one of the ouabain-treated fish was injected intraocularly with BrdU and killed 2 hours later. Sectioned native retina contained, as expected, BrdU-positive cells at the circumferential germinal zone and scattered throughout the outer nuclear layer, corresponding to the positions of rod precursors (data not shown; Johns and Fernald, 1981; Raymond et al., 1988). Sectioned experimental retina also showed BrdU-positive cells at the retinal margin (Fig. 11A), suggesting that a population of proliferative cells continues to reside at the *ora* in ouabain-injected retina, a population that could serve as an ongoing source of new retinal cells (see also Raymond et al., 1988). This peripheral region of experimental retina also contained BrdU-positive cells in the outer nuclear layer, consistent with the expected location of rod precursor cells (Fig. 11A). Central, regenerated retina also displayed BrdU labeling, but BrdU-positive cells were not restricted to the outer nuclear layer, as they would be in central regions of native retina. Rather, a radial stripe of BrdU-labeled cells that spanned all three retinal layers was observed, which was aligned with well-laminated retinal tissue on only one side (Fig. 11B). Sectioned experimental retina from a different fish was processed for indirect immunofluorescence with an anti-PCNA

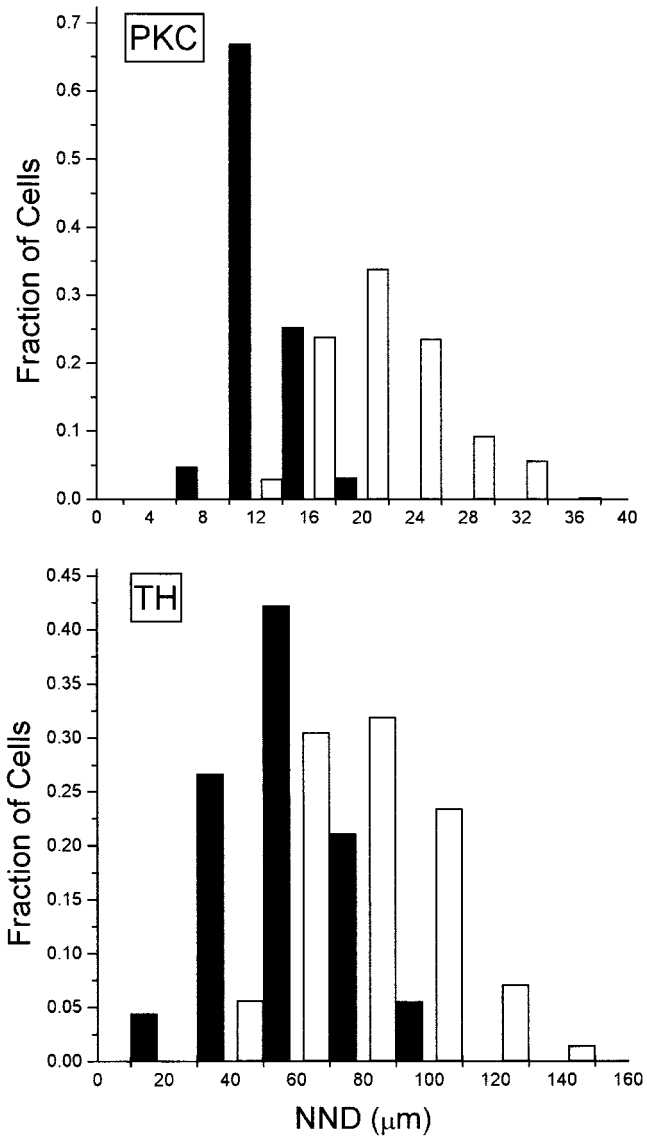

Fig. 10. Nearest-neighbor distance (NND) distributions of tyrosine hydroxylase (TH)-positive and protein kinase C (PKC)-positive cells in native (open bars) and peripheral experimental retina (solid bars). Mean NND values for both cell types are reduced in regenerated retina, and the attendant conformity ratios indicate that the experimental cell mosaics are nonrandom (cf. Tables 2 and 4), but tend toward randomness compared to their counterparts in native retina.

Fig. 9. Inner retinal cells in native and experimental goldfish retina. **a,b:** Radial sections of native and regenerated retina, respectively, screened with an antibody against serotonin. Labeled cells are indicated by arrows. Note the severe disruption in lamination in regenerated retina. **c,d:** Radial sections of native and regenerated retina, respectively, screened with an antibody against tyrosine hydroxylase (TH). Labeled cells are indicated (arrows), as are a region in regenerated retina that appears to contain clusters of cones (asterisk) and other areas that were immunopositive for zpr-1 in nearby sections (arrowheads; see also Fig. 2L). As in (b), the regenerated retina lacks lamination, and the TH-positive cells are distributed in an apparently disorganized manner. **e,f:** TH-positive cells visualized in wholemounts of native (e) and peripheral experimental retina (f). Labeled cells are indicated by black arrows. TH-positive cells are present at relatively elevated density. Additionally, large pigmented objects (white arrow) were commonly observed, and the TH-positive cells were at disparate planes of focus (arrowhead). **g,h:** Protein kinase C (PKC)-positive cells, at the level of synaptic terminals, visualized in whole mounts of native (g) and peripheral experimental retina (h). In native retina, small PKC-positive structures (arrowhead) extend from the principal PKC-positive profiles (arrow). PKC-positive cells are at higher density in peripheral experimental retina. **i:** PKC-positive cells in regenerated retina. The presence of PKC-positive somata (arrowhead) and synaptic terminals (arrow) within the same view is consistent with the disrupted, rippled appearance of this retina. **j:** A region of regenerated retina, containing a large, unidentified, pigmented plexus bordering a plexus-free area (asterisk). Scale bar = 50 mm.

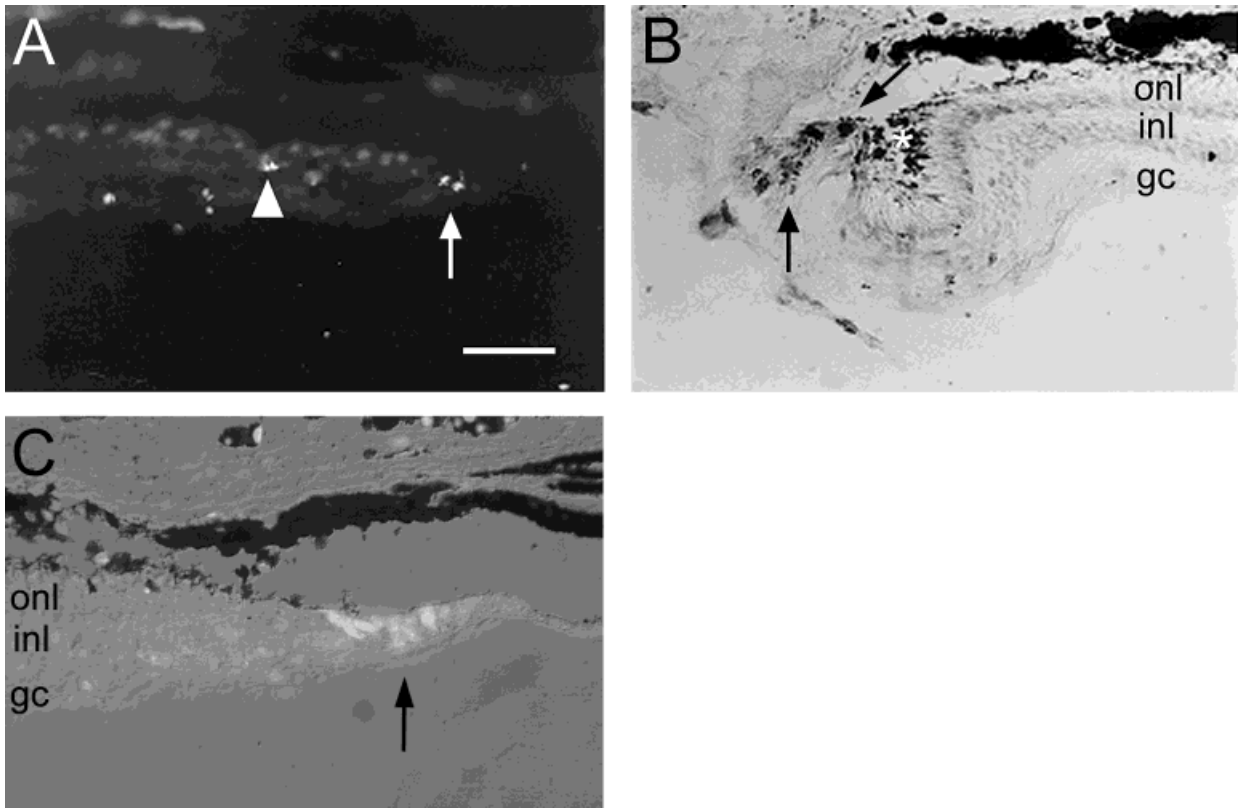

Fig. 11. Proliferative cells in experimental retina. A,B: Experimental eye (Fish 13) was injected with 5-bromo-2′deoxyuridine (BrdU) and fish was killed 2 hours later and processed for indirect immunofluorescence using anti-BrdU. Fluorescent cells in (**A**) lie at the germinal zone (arrow) and in the outer nuclear layer (arrowhead). In (**B**), a region of regenerated retina also contains a germinal zone-like arrangement of cells that incorporated BrdU (radial array of dark cells; indicated by arrows). In this section, anti-BrdU visualization was achieved via a standard horseradish peroxidase/diaminobenzidine protocol (e.g., Cameron and Easter, 1995). Dark color surrounding asterisk is caused by retinal pigmented epithelium melanin. **C:** A different experimental retina (Fish 1), indirect immunofluorescence with anti-proliferating cell nuclear antigen. Labeled (proliferative) cells (arrow) are present in the germinal zone. onl, outer nuclear layer; inl, inner nuclear layer; gc, ganglion cell layer. Scale bar = 50 μm.

monoclonal antibody, and confirmed the presence of PCNA+ proliferative cells at the retinal periphery (Fig. 11C).

DISCUSSION

Retinal regeneration does not recapitulate normal retinal development in quantitative detail: absolute numbers, relative proportions, and mosaic patterns of cells in new retina are not correctly restored. In peripheral ouabain-treated retina, there was a relatively high density of each cone and inner retinal cell type, whereas in regenerated retina, cellular densities were low, and abnormal cellular structures and debris were common. Furthermore, by all quantitative analyses used—NND, DRP, and quadrat analysis—the mosaic patterns of cones and inner retinal cells in peripheral experimental and regenerated retina were statistically different from not just native retina, but also from each other.

Two distinct cone patterns in experimental retina suggest distinct generative mechanisms

The existence of two significantly different, abnormal cell mosaic patterns after ouabain exposure suggests the operation of at least two distinct neurogenerative mechanisms, each different from the mechanisms that operate during normal retinal development and growth. Our results suggest that the major source of peripheral retina is likely to be the circumferential germinal zone at the *ora* (see also Maier and Wolburg, 1979; Raymond et al., 1988). BrdU-incorporation and PCNA experiments suggested that the native germinal zone can survive ouabain exposure, and thereafter repopulate peripheral retina by appositionally adding new retinal cells to the outer rim of the damaged retina, similar to its function in native retina. The appropriate repertoire of cells, including each spectral type of cone (but see Cameron and Powers, 2000), repopulates peripheral retina, suggesting the operation of a mechanism that, as during development, produces all retinal neuronal classes.

However, abnormal densities and proportions of cones (Table 4) indicated a significant disruption in the mechanisms that regulate the generation and/or differentiation of cones after ouabain treatment, even in peripheral retina. The relatively high density of each cell type in peripheral retina could be related to age of the retinal tissue. The mechanisms underlying lifelong growth and expansion of the teleost retina tend to decrease the planimetric density of cones and inner retinal cells (e.g., Johns, 1977; Johns

and Easter, 1977). Therefore, the 6- to 11-month-old peripheral retina might be expected to possess higher densities of cells than contralateral native retina, which is several years older. However, this interpretation cannot explain the abnormal *proportions* of cones consistently observed in peripheral retina.

Another striking abnormality in peripheral experimental retina was evident in the spatial pattern of cells. In native goldfish retina, NND and quadrat analyses revealed that each cone type usually displayed a significant degree of mosaic pattern regularity, and DRP results suggested long-range periodic order. In contrast, these same analyses suggested that each cone type in peripheral experimental retina possessed patterns that tended toward randomness. Furthermore, double NND analysis showed that the spatial correlation between blue and UV cones in native retina was not always present in peripheral experimental retina. Consistent with earlier reports of mechanically injured retina (Cameron and Easter, 1995; Hitchcock and VanDeRyt, 1994; Cameron and Carney, 2000), these results indicate that the mechanisms that organize the genesis and spatial assembly of differentiated retinal cells during growth of peripheral retina subsequent to retinal damage are different from those during normal retinal growth.

The regenerated retinas that were sectioned showed considerable variability in lamination (see Figs. 2C,F,I,L, 9B,D, and 11B), confirming earlier reports that ouabain injections can result in highly variable regenerative responses, perhaps dependent on the degree of initial damage (Maier and Wolburg, 1979; Raymond et al., 1988). However, regenerated retinas studied as whole-mounts displayed consistent and statistically predictable cone mosaic patterns (Table 4). These patterns were typically more clumpy than native or peripheral experimental retina. This observation held for the three cone types examined, with the few exceptions likely caused by analysis difficulties related to low cone density (Grieg-Smith, 1964). We propose that the clumpy cell patterns of regenerated retina reflect the nature of their genesis: spatially disperse neurogenic foci (clusters) generate new retinal cells resulting in spatially disperse cone clumps. Neighboring neurogenic clusters may lack proliferative/regenerative synchrony (Raymond et al., 1988), and/or the cone-free spaces between each clump may represent regions of the original retina where precursor cell survival was poor. Alternatively, regeneration may have proceeded from each neurogenic cluster in a vectorial, radiating manner, from which progressively larger annuli of proliferative cells (or "mini" germinal zones) leave regenerated retinal cells in their "wakes" as they progress outwardly from the original neurogenic source. In this scenario, apparently cone-free regions may represent areas that have not yet experienced retinal differentiation. The BrdU incorporation experiment, showing a germinal zone-like arrangement of proliferative cells at the edge of regenerated retina, was consistent with this interpretation (Fig. 10). However, the relatively broad distribution of zpr-1 labeling in sectioned regenerated retina implies the presence of more cones than were identified in whole mounts reacted for in situ hybridization (cf. Figs. 2L, 3D), suggesting that some neurogenic clusters may generate a restricted set of cell lineages, resulting in clusters of a "preferred" cone type. The lack of spatial correlation between cone types in regenerated retina may support this hypothesis.

Implications for mechanisms of cone mosaic development

Native goldfish retina contains a "square" cone mosaic: each blue cone is surrounded by a symmetric array of four red/green double cones, with UV cones positioned at the corners (Engström, 1960; Marc and Sperling, 1976; Stell and Harosi, 1976; Raymond et al., 1993). Interest in understanding mechanisms for the development of cone mosaics has prompted several recent studies of photoreceptor pattern (Raymond et al., 1993; Robinson et al., 1993; Cameron and Easter, 1993) and differentiation (Raymond et al., 1995; Stenkamp et al., 1996; 1997; Wan and Stenkamp, 2000) in teleost fish. A stereotyped sequence of opsin expression (rod, red, green, blue, then UV) has inspired speculation that the teleost cone mosaic may develop in a manner reminiscent of the *Drosophila* ommatidial mosaic (Heberlein and Moses, 1995), via sequential, cell—cell inductive interactions after the terminal mitoses of cones (Raymond et al., 1995; Stenkamp et al., 1996, 1997). An instructive role for rod photoreceptors in this process (Stenkamp et al., 1996, 1997) has recently been discounted (Wan and Stenkamp, 2000). Nevertheless, sequential inductive/permissive interactions have not been ruled out as mechanisms for regulating the formation of cone mosaics, and studies of retinal regeneration may provide insight into this issue (Cook and Chalupa, 2000). For example, the abnormal cone patterns in regenerated retina may have an analogue in *Drosophila*: when scattered foci of retinal differentiation are experimentally produced in the fly eye, the resultant ommatidia are improperly patterned (Heberlein et al., 1995). The peripheral experimental retina may serve as a more powerful model, however, because the likely source of new cells (circumferential germinal zone) is the same as the source of native retina during normal growth.

Cones in peripheral experimental retina had conformity ratios that met Cook's (1996) criteria for a nonrandom pattern, and one region displayed spatially correlated UV and blue cone mosaics, suggesting that *some* local mechanisms for mosaic assembly may have been preserved or restored. However, quadrat analysis of these same cones suggested random patterns, and spatially correlated UV and blue cone mosaics were not consistently observed, suggesting that local inductive mechanisms are not homogeneously deployed across the growing retina, or that long-range interactions are compromised. Growth at the periphery of ouabain-injected retina is accelerated (Raymond et al., 1988), perhaps allowing insufficient time for patterning interactions. Additionally, the unusual proportions of cone types—which itself reveals a neurogenerative abnormality—may have prevented proper cell—cell interactions, and therefore prevented restoration of normal cone mosaics.

An additional possibility is that cone mosaic formation may be dependent on interactions with a previously generated cone template, which in the case of peripheral experimental retina had been destroyed by ouabain. Supporting this possibility is the observation that, when cells of the germinal zone are selectively killed, the "recovered" germinal zone can produce a well-patterned retina (Wan and Stenkamp, 2000), perhaps reading positional information from nearby undamaged postmitotic retina. However, cone patterning is *not* accurate in retina regenerating subsequent to focal lesions (Braisted et al., 1994;

Cameron and Easter, 1995), where native retina surrounds the lesion and could potentially provide template information. Although some aspects of mosaic pattern formation may involve simple organizing and packing rules (Takesue et al., 1998; Galli-Resta, 1999; Cook and Chalupa, 2000), we hypothesize that a combination of factors, both intrinsic and extrinsic to the circumferential germinal zone, are necessary for development of precise cone patterns.

Implications for recovery of visual function

Visual function can return in goldfish after intraocular injection of ouabain, although both the electroretinogram (ERG) and visual behavior are compromised (Mensinger and Powers, 1999). Such visual deficiencies could arise, in part, from deficiencies noted in regenerated retinal cells (e.g., Cameron and Powers, 2000). The current study suggests that cone mosaic reassembly may be more difficult than the reassembly of inner retinal cell mosaics, implying that cone-derived visual abilities might be particularly compromised in regenerated retina.

However, visual recovery *is* manifest by regenerated retina, suggesting that strategies for inducing neuronal regeneration in damaged mammalian retinas could lead to some recovery in visual function. Retinal regeneration from native sources has not been demonstrated in mammals, but retinal stem cells proximal to the *ora* have been identified (Tropepe et al., 2000), raising the possibility of therapeutic recruitment of new neurons to replace damaged retina in humans. An improved understanding of the mechanisms of cellular differentiation and mosaic assembly during retinal regeneration in teleosts may provide insights for future retinal cell replacement therapies.

ACKNOWLEDGMENTS

This study was supported by National Institutes of Health grants EY12146 (to D.L.S.), EY03352 (to M.K.P.), and EY11160 (to D.A.C.). The authors thank K. Nakanishi and F. Tokunaga for the opsin cDNAs, F. Rosenzweig for suggesting quadrat analysis, and P. Hitchcock for a critical evaluation of the manuscript.

LITERATURE CITED

Barthel LK, Raymond PA. 1990. Improved method for obtaining 3-micron cryosections for immunocytochemistry. J Histochem Cytochem 38: 1383–1388.

Barthel LK, Raymond PA. 1993. Subcellular localization of a-tubulin and opsin mRNA in the goldfish retina using digoxigenin-labeled cRNA probes detected by alkaline phosphatase and HRP histochemistry. J Neurosci Methods 50:145–152.

Boucher SE, Hitchcock PF. 1998. Insulin-related growth factors stimulate proliferation of retinal progenitors in the goldfish. J Comp Neurol 394:386–394.

Braisted JE, Essman TF, Raymond PA. 1994. Selective regeneration of photoreceptors in goldfish retina. Development 120:2409–2419.

Cameron DA, Carney LH. 2000. Cell mosaic patterns in the native and regenerated inner retina of zebrafish: implications for retinal assembly. J Comp Neurol 416:356–367.

Cameron DA, Easter SS Jr. 1993. Cone photoreceptor mosaic of the green sunfish, Lepomis cyanellus. Vis Neurosci 10:375–384.

Cameron DA, Easter SS Jr. 1995. Cone photoreceptor regeneration in adult fish retina: phenotypic determination and mosaic pattern formation. J Neurosci 15:2255–2271.

Cameron DA, Powers MK. 2000. Morphology and visual pigment content of photoreceptors from native and injured goldfish retina. Vis Neurosci 17:623–630.

Cameron DA, Vafai H, White JA. 1999. Analysis of dendritic arbors of native and regenerated ganglion cells in the goldfish retina. Vis Neurosci 16:253–261.

Cook JE. 1996. Spatial properties of retinal mosaics: an empirical evaluation of some existing measures. Vis Neurosci 13:15–30.

Cook JE, Chalupa LM. 2000. Retinal mosaics: new insights into an old concept. Trends Neurosci 23:26–34.

David FN, Moore PG. 1954. Notes on contagious distributions in plant populations. Ann Bot Lond NS 18:47–53.

Dowling JE. 1987. The retina: an approachable part of the brain. Belknap: Cambridge, MA.

Engström K. 1960. Cone types and cone arrangements in the retina of some cyprinids. Acta Zool 41:277–295.

Galli-Resta L. 1999. Modelling the mosaic organization of rod and cone photoreceptors with a minimal-spacing rule. Eur J Neurosci 11:1461–1469.

Grieg-Smith P. 1964. Quantitative plant ecology, 2nd edition. London: Butterworths.

Hauptmann G, Gerster T. 1994. Two-color whole-mount *in situ* hybridization to vertebrate and *Drosophila* embryos. Trends Genet 10:266.

Heberlein U, Moses K. 1995. Mechanisms of *Drosophila* retinal morphogenesis: the virtues of being progressive. Cell 81:987–990.

Heberlein U, Singh CM, Luk AY, Donohoe TJ. 1995. Growth and differentiation in the *Drosophila* eye coordinated by *hedgehog*. Nature 373: 709–711.

Hitchcock PF. 1997. Tracer coupling among regenerated amacrine cells in the retina of the goldfish. Vis Neurosci 14:463–472.

Hitchcock PF, Cirenza P. 1994. Synaptic organization of regenerated retina in the goldfish. J Comp Neurol 343:609–614.

Hitchcock PF, VanDeRyt JT. 1994. Regeneration of the dopamine-cell mosaic in the retina of the goldfish. Vis Neurosci 11:209–217.

Hitchcock PF, Lindsey-Myhr KJ, Easter SS Jr, Mangione-Smith R, Jones DD. 1992. Local regeneration in the retina of the goldfish. J Neurobiol 23:187–203.

Hitchcock PF, Macdonald RE, VanDeRyt JT, Wilson SW. 1996. Antibodies against Pax6 immunostain amacrine and ganglion cells and neuronal progenitors, but not rod precursors, in the normal and regenerating retina of the goldfish. J Neurobiol 29:399–413.

Johnson RL, Grant KB, Zankel TC, Boehm MF, Merbs SL, Nathans J, Nakanishi K. 1993. Cloning and expression of goldfish opsin sequences. Biochemistry 32:208–214.

Knight JK, Raymond PA. 1990. Time course of opsin expression in developing rod photoreceptors. Development 110:1115–1120.

Larison KD, BreMiller R. 1990. Early onset of phenotype and cell patterning in embryonic zebrafish retina. Development 109:567–576.

Levine EM, Hitchcock PF, Glasgow E, Schechter N. 1994. Restricted expression of a new paired-class homeobox gene in normal and regenerating adult goldfish retina. J Comp Neurol 348:596–606.

Maier W, Wolburg H. 1979. Regeneration of the goldfish retina after exposure to different doses of ouabain. Cell Tissue Res 202:99–118.

Marc RE, Sperling HG. 1976. The chromatic organization of the goldfish cone mosaic. Vision Res 16:1211–1224.

Mensinger AF, Powers MK. 1999. Visual function in regenerating teleost retina following cytotoxic lesioning. Vis Neurosci 16:241–251.

Raymond PA, Hitchcock PF. 2000. How the neural retina regenerates. In: Fini ME, editor. Vertebrate eye development. New York: Springer-Verlag. p 197–218.

Raymond PA, Reifler MJ, Rivlin PK. 1988. Regeneration of goldfish retina: rod precursors are a likely source of regenerated cells. J Neurobiol 19:431–463.

Raymond PA, Barthel LK, Rounsifer ME, Sullivan SA, Knight JK. 1993. Expression of rod and cone visual pigments in goldfish and zebrafish: a rhodopsin-like gene is expressed in cones. Neuron 10:1161–1174.

Raymond PA, Barthel LK, Curran GA. 1995. Developmental patterning of rod and cone photoreceptors in embryonic zebrafish. J Comp Neurol 359:537–550.

Raymond Johns P. 1977. Growth of the adult goldfish eye. III. Source of the new retinal cells. J Comp Neurol 176:343–358.

Raymond Johns P, Easter SS Jr. 1977. Growth of the adult goldfish eye. II. Increase in retinal cell number. J Comp Neurol 176:331–342.

Raymond Johns P, Fernald RD. 1981. Genesis of rods in teleost fish retina. Nature 293:141–142.

Ripley BD. 1981. Spatial statistics. New York: John Wiley & Sons.

Robinson J, Schmitt EA, Harosi FI, Reece RJ, Dowling JE. 1993. Zebrafish ultraviolet visual pigment: absorption spectrum, sequence, and localization. Proc Natl Acad Sci USA 90:6009–6012.

Rodieck RW. 1991. The density recovery profile: a method for the analysis of points in the plane applicable to retinal studies. Vis Neurosci 6:95–111.

Schultz K, Goldman DJ, Ohtsuka T, Hirano J, Barton L, Stell WK. 1997. Identification and localization of an immunoreactive AMPA-type glutamate receptor subunit (GluR4) with respect to identified photoreceptor synapses in the outer plexiform layer of goldfish retina. J Neurocytol 26:651–666.

Skellam JG. 1952. Studies in statistical ecology. I. Spatial pattern. Biometrika 39:346–362.

Stell WK, Harosi FI. 1976. Cone structure and visual pigment content in the retina of the goldfish. Vision Res 16:647–657.

Stenkamp DL, Hisatomi O, Barthel LK, Tokunaga F, Raymond PA. 1996. Temporal expression of rod and cone opsins in embryonic goldfish retina predicts the spatial organization of the cone mosaic. Invest Ophthalmol Vis Sci 37:363–376.

Stenkamp DL, Barthel LK, Raymond PA. 1997. Spatiotemporal coordination of rod and cone photoreceptor differentiation in goldfish retina. J Comp Neurol 382:272–284.

Stenkamp DL, Frey RA, Prabhudesai SN, Raymond PA. 2000. Function for *hedgehog* genes in zebrafish retinal development. Dev Biol 220: 238–252.

Stuermer CAD, Niepenberg A, Wolburg H. 1985. Aberrant axonal paths in regenerated goldfish retina and tectum following intraocular injection of ouabain. Neurosci Lett 58:333–338.

Sullivan SA, Barthel LK, Largent BL, Raymond PA. 1997. A goldfish *Notch-3* homologue is expressed in neurogenic regions of embryonic, adult, and regenerating brain and retina. Dev Gen 20:208–223.

Suzuki S, Kaneko A. 1990. Identification of bipolar cell types by protein kinase-c-like immunoreactivity in the goldfish retina. Vis Neurosci 5:223–230.

Takesue A, Mochizuki A, Iwasa Y. 1998. Cell-differentiation rules that generate regular mosaic patterns: modelling motivated by cone mosaic formation in fish retina. J Theor Biol 194:575–586.

Tropepe V, Coles BL, Chiasson BJ, Horsford DJ, Elia AJ, McInnes RR, van der Kooy D. 2000. Retinal stem cells in the adult mammalian eye. Science 287:2032–2036.

Wan J, Stenkamp DL. 2000. Cone mosaic development in the goldfish retina is independent of rod neurogenesis and differentiation. J Comp Neurol 423:227–242.

Wässle H, Riemann HJ. 1978. The mosaic of nerve cells in the mammalian retina. Proc R Soc Lond B Biol Sci 200:441–461.

Yazulla S, Zucker CL. 1998. Synaptic organization of dopaminergic interplexiform cells in the goldfish retina. Vis Neurosci 1:13–29.